NATIONAL ADVISORY COMMITTEE FOR AERONAUTICS

TECHNICAL NOTE 4338

GRAPHS OF REDUCED VARIABLES FOR COMPUTING HISTORIES OF VAPORIZING FUEL DROPS, AND DROP HISTORIES UNDER PRESSURE

By G. L. Borman, M. M. El Wakil, O. A. Uyehara, and P. S. Myers
University of Wisconsin

NACA

Washington

September 1958

TABLE OF CONTENTS

NATIONAL ADVISORY COMMITTEE FOR AERONAUTICS

TECHNICAL NOTE 4338

GRAPHS OF REDUCED VARIABLES FOR COMPUTING HISTORIES OF VAPORIZING FUEL DROPS, AND DROP HISTORIES UNDER PRESSURE

By G. L. Borman, M. M. El Wakil,
O. A. Uyehara, and P. S. Myers

SUMMARY

The purpose of the present investigation was two-fold. The first objective was to obtain a simplified calculation technique that would replace the complicated automatic computer calculations. The second objective was to obtain experimental data for single droplets vaporizing at pressures greater than 1 atmosphere and to check computed histories against these data.

A method of calculation using reduced curves and nomograms is explained. Graphs and nomograms that can be used to calculate histories of n-decane droplets are presented. Similar graphs may be constructed for any pure fuel with known physical properties, as described in this report. The accuracy of the calculation technique is shown to be within the agreement between experiment and theory. The method of application of such simplified calculations to fuel sprays is discussed, and the limitations of the calculations are pointed out.

Steady-state temperatures of hexane, decane, and hexadecane were obtained experimentally for various temperatures and pressures from 1 to 5 atmospheres. The experimental data agreed with the calculated values to within $\pm 10^{\circ}$ R. A few experimental unsteady-state histories for n-decane at 2 and 4 atmospheres pressure are presented. These histories show no great deviation from the calculated histories.

INTRODUCTION

An understanding of the processes that occur in the atomization, acceleration, and vaporization of fuel droplets in a spray is important to the design of combustors. Atomization results in breaking the mass of the liquid fuel into a spray of tiny spherical droplets and thus tremendously increases the fuel surface area exposed to the air. The total mass vaporized from the spray may then be obtained from a study of the vaporization of each droplet, or a number of individual droplets, in the spray. Since rapid vaporization is essential to ensure a rapid rate of heat release, an understanding of the phenomena occurring in the spray is important. In addition, if the largest droplets do not have time to vaporize sufficiently, they may leave the combustion zone in liquid

form; this represents a loss in efficiency charged against the combustor. Thus, it is of interest to be able to estimate rapidly the histories of single droplets in order to approximate spray histories.

Earlier investigations at the University of Wisconsin were concerned with the problem of predicting the temperature and mass histories of single droplets. A theoretical investigation (ref. 1) showed the effects of the unsteady-state portion of the vaporization histories to be of considerable importance. The theoretical study was followed by an experimental study (refs. 2 and 3) primarily concerned with vaporization under atmospheric pressure. Liquid-fuel droplets were hung on a spherically shaped thermocouple junction. Heated air was then suddenly caused to flow over the drop. The temperature and size of the drop were recorded as a function of time. The experimental results were compared with computed histories; theoretical and experimental mass curves agreed to within 20 percent.

The investigation reported herein is concerned with two fundamental problems. The first problem is to compare the theoretical predictions with experimental data taken at pressures higher than 1 atmosphere. The second problem is to evolve a simplified calculation technique that can be used to obtain droplet histories easily. The equations for heat transfer, mass transfer, and aerodynamic drag may thus be solved simultaneously to result in a reasonably simple and accurate method of predicting spray vaporization behavior. It should be noted that such calculations give no information concerning the possible chemical interaction between fuel and air, nor do they take into account the effect on the vaporization of any fuel vapor that may be mixed with the air (refs. 3 and 4). These latter problems are. however, beyond the scope of the study of single-droplet vaporization.

This investigation was carried out at the University of Wisconsin under the sponsorship and with the financial assistance of the National Advisory Committee for Aeronautics. Special acknowledgment is given to Mr. Wolfgang Rockenhauser for his help in obtaining some of the pressure data presented herein.

SYMBOLS

A_0	surface area of liquid drop
C	lumped physical parameter (table I)
$C_{p,a}$	specific heat of air at constant pressure
$C_{p,f}$	specific heat of fuel vapor at constant pressure

$C_{p,L}$	specific heat of liquid fuel
$C_{p,m}$	specific heat of air-vapor mixture
D	lumped physical parameter (table I)
D_v	diffusion coefficient of air-vapor system
F(X)	integral function of X
$g(T_w)$	lumped physical parameter
h	coefficient of heat transfer
$K(T_w)$	lumped physical parameter
K_a	thermal conductivity of air
K_f	thermal conductivity of fuel vapor
K_m	average thermal conductivity in air-vapor mixture
$\bar{M}$	mean molecular weight
M_a	molecular weight of air
M_f	molecular weight of fuel
m	mass of drop at time θ
Nu'	Nusselt number for mass transfer
$P_{f,L}$	liquid vapor pressure
Pr	Prandtl number
P_T	total pressure
Q_L	heat received at drop surface
Q_v	heat-transfer rate
Q_λ	heat of vaporization
q_1	first dummy scale on θ_t' nomogram
q_2	second dummy scale on θ_t' nomogram

Re	Reynolds number
R_f	gas constant for fuel
r	radius
Sc	Schmidt number
s	dummy variable
T_B	air temperature
T_L	liquid temperature
T_m	mean temperature
T_w	steady-state liquid temperature
V	air velocity relative to drop
X	(Nu' - 2)
z	physical parameter (appendix D)
θ	time, sec
θ_t	total droplet vaporization time
θ_t'	total droplet vaporization time for drop initially at steady-state conditions
μ_a	viscosity of air
μ_f	viscosity of fuel vapor
μ_m	mean viscosity of air-vapor mixture
ρ_a	density of air
ρ_L	density of liquid
ρ_m	mean density
λ	latent heat of vaporization
ω	mass vaporization rate from drop

Subscripts:

a	air
d	decane
f	fuel
L	liquid
m	mean value
u	unsteady-state condition
w	steady-state condition
0,1,2, . . .	0, initial value; 1,2, . . . following values or increments

Superscript:

*	reduced value of variable, a dimensionless quantity

EXPERIMENTAL INVESTIGATION

Experimental Apparatus

The basic components of the experimental apparatus described in reference 3 were retained for the experiments at elevated pressure (fig. 1). A description of the optical system, air heater, and temperature recorder is found in reference 3 and, for the most part, is not repeated herein.

The major addition to the previously used apparatus was a pressure bomb or flow chamber, which was fastened to the air heater and enclosed the air nozzle located at the bottom of this chamber. A throttled port at the top of the chamber allowed the outward airflow to be regulated. By proper adjustment of the line pressure, inlet flow, and exit flow, a range of air pressures and flow velocities could be achieved. The thermocouple (fig. 2) extended down into the chamber from the top and could be adjusted so that the thermocouple bead was located immediately above and at the center of the air nozzle. The airflow over the thermocouple bead was controlled by an externally triggered deflecting plate.

The static air pressure in the chamber was measured with three calibrated pressure gages whose maximum ranges were 15, 30, and 60 pounds per square inch gage, respectively.

The air velocity at the liquid droplet was measured with an Illinois Testing Laboratories Velometer having a range of 0 to 600 feet per minute. Since this velometer was designed to operate at atmospheric pressure, the velometer case and tubes had to be maintained at the same pressure as that of the airstream whose velocity was being measured. Since the velometer could not withstand prolonged periods in a hot atmosphere, it was necessary to enclose the velometer in a separate housing. The static pressure within this housing was made equal to that in the chamber by means of an interconnecting tube. A pressure gage mounted on the velometer housing was used to compare housing and chamber pressures. The metal probes of the velometer were introduced into the chamber through a bushing and could be slid over the nozzle or made flush with the inside wall of the chamber. The interconnecting tube, probes, and brackets were all water-cooled so that the velometer housing remained cool despite the elevated temperature of the chamber.

The optical system was not revised for taking pressure data except that the second condensing lens and the f/16 projection lens were placed inside the bomb. Two 1-inch-thick glass windows made up two walls of the bomb and thus allowed the light beam to pass through the bomb. A small mirror was mounted outside the bomb in such a way as to allow the inside of the bomb to be observed directly.

At 1 atmosphere the fuel droplet could be placed directly on the thermocouple, as described in reference 3. For data taken at elevated pressures a more elaborate system was required. This system is shown in figure 3. The fuel was contained in the piston device shown in the figure. A fine and coarse thread allowed adequate control of the feed. Since the piston device was external to the chamber, fuel changes could be made without disturbing the air pressure in the chamber. It was found necessary to cool the fuel by means of a water jacket so that no vaporization or heating of the fuel would occur in the fuel line. Without this cooling, heat conducted from the bomb would vaporize the fuel before the drop could be suspended on the thermocouple bead. The hypodermic needle could be brought up to the thermocouple by means of the threaded disk shown in figure 3. The needle could be drawn back most rapidly by manually sliding the entire fuel line and water jacket back an inch or two. When changing fuels, it was necessary to wash the entire fuel system carefully with acetone before introducing the new fuel.

Numerous attempts were made to add cool air to the chamber either prior to or during the experiment. It was thought that such subsidiary air would help to cool the thermocouple and fuel prior to taking the history. None of these attempts was fully successful. Any air introduced at the sides or bottom of the chamber caused fluctuations in temperature and velocity at the test section. A method was devised to turn on the subsidiary air and simultaneously open an additional air release

port. This method prevented disturbance of the air pressure and temperature but caused a disturbance of the velocity that lasted approximately 30 seconds after the cool air was turned off. Since the cooling effects lasted only slightly longer than the velocity disturbance, this method was impractical.

Procedure and Accuracy

The first step in taking experimental data was to calibrate the optical system as described in reference 3. After this calibration, the thermocouple was placed in the bomb, and the system was brought up to the desired temperature and pressure. The system usually required 24 hours of heating to establish a constant air temperature. Before data were taken, the air velocity and pressure were measured and recorded. The pressure measurements had a relative error of less than 2 percent. The air temperature was measured by using the thermocouple itself. The thermocouples were calibrated in a hot oil bath prior to being used; this calibration was accurate to within $\pm 2^{\circ}$ R. The procedure in taking data consisted of the following actions: Slowly bringing the hypodermic needle up to the bead, placing the drop on the thermocouple, pulling back the needle quickly, starting camera and recorders, and triggering the air blast. Accuracy and calibration data for the recorder, film, and temperature readings may be found in reference 3.

Several runs usually were made with the same fuel to check reproducibility. The unsteady-state portion of the histories proved to be less reproducible than would be desired. The thermocouple became heated because of the continued flow of hot air in the confined space of the bomb prior to taking the history. This heating, together with entrapped air bubbles in the drop, caused the initial portion of the temperature curve to vary considerably from run to run. Repeated trials produced curves believed to be reasonably accurate in the unsteady-state portion of the history, but the difficulties of the experiment prevented the taking of data that could be considered as reliable as that presented in reference 3. Reproducibility of steady-state temperatures was found to be good, with variations as small as $\pm 3^{\circ}$ R.

Experimental Results

A limited amount of acceptable data was obtained for pressures greater than 1 atmosphere. Several trends, however, were experimentally established. As the pressure is increased, the unsteady-state becomes even more important; that is, the ratio of the time to attain the steady-state temperature to the time to completely vaporize the drop increases. Theoretically, this ratio approaches a limit of 1 as the pressure is increased. Secondly, the steady-state temperatures increase with increasing pressure. This increase tends to become less at higher pressures, so that the difference between unsteady-state temperatures at 1 and 2 atmospheres is much greater than the difference at 4 and 5

atmospheres. Thirdly, the higher steady-state temperatures may in some cases cause the total vaporization time to decrease with increasing pressure.

Figures 4 and 5 show experimental temperature and mass histories at 2 and 4 atmospheres of pressure. Figure 6 gives experimental steady-state temperatures for various pressures against air temperature. At higher air temperatures, heat transfer from the thermocouple wires caused the liquid temperatures to be erroneously high. This heat-transfer problem was increased at higher pressures because the thermocouple itself was heated more in the bomb than when in open air.

5080

Comparisons of Experimental and Calculated Results

Figure 6 shows the agreement between calculated and experimental steady-state temperatures. This agreement is within $\pm 10^{\circ}$ R as compared with $\pm 4^{\circ}$ for 1 atmosphere of pressure. About $\pm 5^{\circ}$ of this difference may be accounted for by experimental inaccuracies. Figures 4 and 5 show both computed and experimental histories at 2 and 4 atmospheres. The same error trends that were discussed in reference 3 are present; that is, the experimental and mass-transfer histories were within 20 percent for all cases studied. With the exception of steady-state temperature agreement, the agreement between experimental and calculated histories was similar to that reported in reference 3. No other significant error trend was found as the pressure was increased to 5 atmospheres absolute.

SIMPLIFIED CALCULATION TECHNIQUE

Original computations of droplet vaporization histories, as found in references 1 to 3, were performed with the aid of either desk calculators or automatic high-speed computers. The desk calculations were prohibitively lengthy. The time required to compute histories with sequenced computers varied considerably with the type of machine available. The IBM 650 with subroutined floating decimal can calculate a history in approximately 10 minutes. Other machines may require as much as 1/2 hour or as little as 2 minutes to calculate a history.

While the high-speed computer is an excellent tool for calculation, it has a number of disadvantages: Computer programing may be time consuming, computer time may be difficult to obtain, the cost of operation is high, and lastly a computer of adequate size simply may not be available. Therefore, an attempt was made to replace the computer calculations with a simplified calculation technique. A number of techniques were tried with little success; these attempts are reported in appendix A. The method of reduced-variable graphs, which proved most successful, is described herein.

Construction of Plots of Reduced Variables

The mass-transfer histories given in reference 3 are quite similar in appearance, the characteristics curve being "S" shaped. Deviation from this shape occurs only when the initial slope is not approximately zero. Such deviations may be eliminated by restricting the initial liquid temperature to some appropriately low value. The exact value of the liquid temperature that will satisfy this condition depends on the fuel and air temperature range. For example, the maximum initial liquid temperature for n-decane with air temperatures of 800° to 1600° R that will give an initial slope of approximately zero is 550° R. This maximum temperature is called the zero-slope temperature.

With the initial temperature fixed at the zero-slope value, all histories for a particular fuel are similar in appearance except for the time scale. For a particular fuel under the conditions studied, division of the time scale by the total vaporization time gives a family of reduced-mass curves that all lie within 20 percent of each other. If the air temperature is held constant and the radius and/or velocity varied, the reduced curves fall very close to each other. Variation of the air temperature thus causes most of the 20-percent variation mentioned.

Examination of the mass curves shows that the inflection point corresponds to the end of the unsteady state. The proportion of time spent in the unsteady state is known to be influenced by the air temperature. Fortunately, the reduced-mass curve is nearly a straight line in the neighborhood of the inflection point and thus minimizes the effects of air temperature. A single curve thus can be made to represent all such reduced curves to within the accuracy warranted by the agreement between IBM calculations and experiment. Such a reduced curve for n-decane is shown in figure 7(a). This curve was constructed from computed mass-transfer curves. When the reduced curve was drawn, points farther to the right were favored so as to fit the experimental trends better, as discussed in reference 3.

Computations for initial liquid temperatures lower than the zero-slope temperature offer no difficulty. To a good approximation the equation for heat transfer with no mass transfer applies to these low liquid temperatures. Appendix A gives the equation and solution for this case.

Computations for initial liquid temperatures higher than the zero-slope temperature require the use of only part of the reduced-mass-transfer curve. The portion of the reduced-mass-transfer curve to the right of any value of reduced time corresponds to a mass history with initial temperature greater than the zero-slope temperature. If the liquid temperature at each reduced time is known, the reduced-mass-transfer history may be obtained by merely taking that part of the history to the right of the point corresponding to the desired initial temperature. New reduced axes that run from 0 to 1 must then be constructed so that the history will begin at zero time and zero mass transferred.

A plot of liquid temperature against time gives a single curve for any one fuel, pressure, and air temperature; that is, the curve is independent of size and velocity. Families of curves must be drawn for various pressures and temperatures. Figure 7(b) gives such curves for n-decane at 1 atmosphere of pressure. Again, the curves were constructed from computed data. A reduced-temperature scale does not bring these curves for various air temperatures together.

The total vaporization time may be obtained from steady-state vaporization time and the reduced-mass curve, as explained in the following section. As a computational aid, the graphs and nomogram presented in figures 8 to 10 were constructed from equation (A1) and the physical properties given in appendix IV of reference 3. Appendix B gives details concerning the construction of figure 10.

Graphs and nomograms similar to those given here may be constructed for any pure hydrocarbon fuel. Hexane and hexadecane, for example, were reduced in the same manner as decane. Unfortunately, the shape of the reduced-mass curve varies with the fuel. No single curve that would represent all fuels could be found. When the curves for various fuels are plotted so as to agree during the initial portion, they diverge at higher values of the reduced time θ^*.

If it is desired to calculate a mass history for a fuel "x" similar to decane (i.e., the steady-state temperatures are within approximately 50° R of each other for several air temperatures), the reduced-mass curve for decane may be corrected as follows: Use the reduced curves for decane with the initial liquid temperature computed from the equation

$$T_{L,0,d} = T_{L,0,x} + (T_{w,d} - T_{w,x})$$

where $T_{L,0,d}$ is the initial liquid temperature to be used for decane, $T_{L,0,x}$ is the initial liquid temperature of fuel "x," $T_{w,d}$ is the steady-state temperature for decane, and $T_{w,x}$ is the steady-state temperature for fuel "x." The construction of the reduced curve follows the procedure given in the following section. The total vaporization time should be calculated from data for fuel "x." It should be remembered that this correction gives only an approximation to the correct reduced curve and should be used only for fuels similar to decane.

The reduced-mass curve for decane at 1 atmosphere pressure may be used with but little error for higher pressures up to at least several atmospheres. The liquid-temperature curves will not be the same for different pressures.

Calculation of Mass and Temperature Histories Using Plots of Reduced Variables for Droplets Vaporizing with Constant Relative Air Velocity

Figure 7(a) is a plot that represents all mass-transfer curves (within the accuracy given on p. 14) for the following range of conditions:

Initial liquid temperature, $^{\circ}R$	550
Air temperature, $^{\circ}R$	$800 \leq T_B \leq 1600$
Air velocity, in./sec	$10 \leq V \leq 1000$
Initial radius, in.	$4 \times 10^{-4} \leq r_0 \leq 10^{-2}$
Fuel	n-decane
Total pressure, atm abs	$1 \leq P_T \leq 4$

Figure 7(b) is a plot of liquid temperature against reduced time for various air temperatures. Each curve is for 1 atmosphere of total pressure and the given range in radius and velocity.

Two steps are involved in the calculation of mass histories from the charts. Step 1 is the construction of a reduced-mass curve appropriate to the initial liquid temperature of interest. Step 2 is the conversion of the reduced curve to the desired mass (against time) history. The procedures to be used in different cases are indicated as follows:

Step 1: Construction of reduced-mass curves

(a) $T_{L,0} = 550^{\circ}$ R

Drops with initial liquid temperature of 550° R have the reduced-mass-transfer curve given by figure 7(a).

(b) $T_{L,0} > 550^{\circ}$ R

If the initial liquid temperature is greater than 550° R, only a part of the reduced-mass curve given in figure 7(a) can be used. The construction of the new reduced-mass curve for this case proceeds as follows:

(1) Select from figure 7(b) the curve corresponding to the air temperature of interest.

(2) Read the value of θ^* given by this curve at the temperature $T_{L,0}$; call this value of the reduced time θ^*_0.

(3) Find the point corresponding to θ_0^* on the curve of figure 7(a); call this point (m_0^*, θ_0^*).

(4) Let the point (m_0^*, θ_0^*) be the origin of a new set of axes; these axes should be constructed parallel to the original m^*, θ^* axes. Construct scales on each of these new axes that run from 0 to 1.0. The value 1 should coincide with the value 1 on the old m^*, θ^* axes. Figure 11 is a schematic example of such a construction. The new axes and the portion of the reduced-mass curve to the right of the new origin (m_0^*, θ_0^*) form the reduced-mass curve sought. The uniform scales (fig. 12) can be used in constructing the new axes scale, or a straight edge and the geometry of similar triangles can be used in place of the uniform scales.

(c) $T_{L,0} < 550^\circ$ R

If the initial liquid temperature is less than 550° R, the portion of the mass history prior to 550° R must be computed separately. Since no mass is transferred during this period, the calculation is for the heating time only. This case proceeds as follows:

(1) Use equation (A2c) with values of C and D as given in table I to calculate the time required to reach 550° R liquid temperature. Note that this is not a reduced time.

(2) Calculate the actual mass history from 550° R on as directed in step 1(a) and step 2.

(3) Add the time to reach 550° R (step 1(c1)) to the result of step 1(c2).

Step 2: Conversion of reduced-mass curves to actual-mass histories

The reduced-mass curve given by step 1 is converted to a mass-transfer history by multiplying the reduced time θ_0^* by the total vaporization time θ_t, which is obtained as follows:

Pick a value of θ^* that is well within the steady-state region (say $\theta^* = 0.8$); call this point (m_w, θ_w). Find the reduced radius $r_w^* = r_w/r_0$ corresponding to this point by use of figure 13. Figure 13 requires the knowledge of $T_{L,0}$, T_w, and m_w^*, all of which are known. Figure 10 now gives the vaporization time for a drop vaporizing at steady-state conditions with initial radius r_w and velocity V. The value of θ_t can now be calculated from the equation

$$\theta_t = \theta_t'/1 - \theta_w^*$$

A numerical example of this procedure is given in appendix C.

Construction of Mass Histories for Droplets Vaporizing with Changing Relative Air Velocity

It is assumed that drag coefficients are available from which the relative air velocity may be calculated (see ref. 5). The procedure to be followed is a stepwise trial-and-error process:

(1) Construct the reduced-mass-transfer graph as in step 1 of the preceding section.

5080

(2) Hold all conditions except velocity constant and calculate values of θ_t for various V. The calculation is performed as in step 2 of the preceding section.

(3) Pick an increment of time $\Delta\theta$ that is some small fraction of the θ_t value corresponding to the given initial velocity.

(4) Assuming the mass to be constant, calculate the velocity at time $\Delta\theta$ as predicted by the drag equations. Calculate the average velocity during time $\Delta\theta$.

(5) From the graph prepared in step (2) of this section, read the value of θ_t corresponding to the average velocity calculated in step (4). Call this time $\theta_{t,1}$.

(6) Calculate $\Delta\theta_1^* = \Delta\theta/\theta_{t,1}$.

(7) From the mass curve of step (1) of this section, find the m_1^* corresponding to $\Delta\theta_1^*$. This gives the first point, $(m_1^*, \Delta\theta)$, of the mass history.

(8) If the mass has changed appreciably during the time $\Delta\theta$, the calculations of steps (4) to (7) may need to be repeated with a more accurate average mass.

(9) Repeat steps (4) and (5) for the next time step. Step (6) now should read $\Delta\theta_2^* = \Delta\theta_1^* + \Delta\theta/\theta_{t,2}$. Step (7) follows as before.

For steps other than the first, the curves for velocity and mass of the drop may be extrapolated as an aid in estimating the values to be used for the next step.

The calculation thus proceeds step by step to give the mass-transfer history. A numerical example is given in appendix C.

Accuracy of Method of Reduced-Variable Charts

Ease of calculation and speed are important factors in considering the relative merits of calculation techniques, but the accuracy of the results must not be ignored. The range of conditions covered by the reduced-variable plots was chosen so as to approximate engine operating conditions. This range exceeded the range for which experimental data were available. Direct comparison of mass histories obtained by use of the reduced-variable charts and the experimental curves was possible only for the largest drop size in the range considered, that is, 500 microns. Comparisons of experimental curves with curves obtained from IBM calculation and from the reduced-variable charts are given in figure 14. Curves for calculations assuming no unsteady state and also for the method of solid spheres (see appendix A) are included. In each case the use of the reduced-variable charts provides the best agreement with experiment. In order to check these charts for a wider range of conditions, comparisons with IBM calculations only are given in figure 15. In each case the agreement is good. In general the agreement is poorest at low air temperatures. Radius and velocity have but little effect on the relative error. While the charts agree with the IBM calculations for these conditions, it must be remembered that the theoretical calculations themselves are subject to the error trends given in reference 3. These trends suggest that the IBM calculations may disagree considerably with experiment for very small droplets.

Figure 16 compares the results of calculations using the IBM and the reduced-variable charts for variable air velocity. The velocity curve was chosen arbitrarily and thus was known precisely. This procedure is permissible, since the computations were for comparison purposes only.

Use and Limitations of Histories

In order to use the computed histories to predict the behavior of an air-spray system, the following technique may be used:

(1) A representative droplet-size distribution for the condition of interest is determined or assumed. The initial liquid temperature must be known or assumed. The airflow pattern and relative air velocity must also be known or assumed.

(2) The use of the computed histories that assume no interaction between droplets should be justified on the basis of the dispersion of the spray in question and the over-all fuel-air ratio. In the case of sprays found in jet engines, the authors believe that this assumption is justified and that the computations presented are adequate. If the spray is dense, other considerations and techniques will have to be taken into account (refs. 3 and 4).

(3) The entire spray may then be divided into a number of "size groups" and the percentage by weight of each determined. Each size group may be represented by a single droplet size that may be chosen as some average of the range of its particular size group. Any error involved in the averaging technique will be minimized if a sufficiently large number of groups is chosen.

(4) Each representative droplet will be treated in the manner suggested in this report. Since the droplets will be affected by aerodynamic drag, the procedure outlined on page 13 should be used.

5080

(5) The amount vaporized from each size group will then be obtained as a function of the distance from the nozzle or the point at which the spray was first formed and came into contact with the air.

(6) The total amount of vapor formed from the spray can then be obtained by adding the properly weighted vaporization due to each size group.

(7) After the initial fuel-air ratio by weight is known, a distance from the nozzle may be found at which an over-all air-vapor mixture of combustible strength is formed and where all physical processes are thought to have made their contributions. A spark plug or flameholder may then be placed near that point to initiate or sustain combustion. The balance of the computed individual histories are actually meaningless beyond this point.

The calculated vaporization histories do not necessarily describe the droplet lifetimes in their entirety. Some or all the droplets present, say in a fuel-spray system, may deviate from these calculated histories sometime during their lifetimes in an actual combustor. The lifetimes of fuel droplets may be thought of as composed of two parts. The first is physical; this can be adequately described by the calculated vaporization histories obtained by using the technique presented in this report. The second is chemical; this includes the time required for the oxygen and fuel molecules to arrange themselves for combination into combustion products. It is quite likely that the two mentioned parts, physical and chemical, overlap to an appreciable degree.

A second limitation has to be placed on the unrestricted use of the computed histories as previously outlined. These computations are based on the assumption that an abundant quantity of air accompanies each droplet; that is, no interaction occurs between droplets, and the pressure and temperature of the air are unaffected by the vaporization process. Thus the computed histories do not show any effect that may result from the close proximity of droplets. In dense parts of a spray the air temperature may drop appreciably. The rate of vaporization

also will decrease because of the reduction of diffusional driving forces by the presence of fuel vapor in the air surrounding the droplets. As an ultimate condition, the fuel-air system will reach adiabatic equilibrium, and the vaporization process ceases (refs. 3 and 4).

It is felt that, for the most part, fuel sprays existing in continuous flow or jet-type combustors are so dispersed that the partial pressure of the fuel vapor in the air surrounding the droplets is not high enough to affect the diffusional driving forces appreciably. The driving force, therefore, will always be assumed equal to the fuel vapor pressure of the liquid fuel at the liquid temperature. The droplets are far enough removed from each other that "single droplet" computations, such as those described in this and previous reports, are accurate enough to describe the histories of the droplets during their period of pure vaporization; that is, before ignition takes place. The air temperature during this process will not be appreciably reduced. The air pressure will remain uniform, since frictional losses and the pressure rise due to vaporization are relatively negligible.

Caution should also be exercised in the use of "ignition delays" or "preflame distances" obtained by using one of these procedures. In actual combustors, there are a number of variables that render this procedure comparative at best. Turbulence and backflow, for example, disturb the pattern of relative velocity between air and drops. Atomization uncertainties are also of concern. Heat transfer by radiation from the combustor walls and flame to the liquid droplets adds to the convective heat transfer to the droplets and is difficult to evaluate. The evaluation just given should, therefore, be used for estimation or comparison purposes only.

CONCLUSIONS

An investigation was conducted to (1) compare the theoretical predictions with experimental data obtained at pressures from 1 to 5 atmospheres, and (2) evolve a simplified calculation technique of reduced-variable graphs and nomograms so as to obtain droplet histories easily. The results and conclusions are stated as follows:

1. The ratio of the unsteady-state time to the total vaporization time increases with increasing pressure. It is conceivable that at very high pressures the entire droplet lifetime may be spent in the unsteady state.

2. Agreement between calculated and experimental mass-transfer histories was within 20 percent for all cases studied. Reasonable agreement between theory and experiment was found for pressures up to 4

atmospheres. Extrapolation of the trends of agreement between experiment and theory suggests that the theory may be in serious disagreement with experiment for droplets considerably smaller than 250 microns initial diameter.

3. The experimental method is definitely limited in scope. This method ceases to be practicable for very small drops or higher air velocities. Small droplets imply such short vaporization times that it is impossible to place the drops on the thermocouple before they vaporize. In addition, the time to develop the airstream profile may become important and thus raise the uncertainties of turbulence and air-velocity magnitude. Air velocities are limited by the effects of droplet distortion and blowoff. It is conceivable that the method may be used for higher air temperatures or pressures but only with considerable experimental difficulty. It may be concluded that some other method should be sought if conditions greatly different from those studied herein are to be considered.

4. The method of reduced-variable charts presented in this report is simple enough and accurate enough to be used for the calculation of the vaporization of sprays. The method provides as much accuracy as is warranted by the agreement between theory and experiment.

5. Many uncertainties in the application of these studies to fuel sprays result from a lack of understanding of the detailed behavior of sprays. Drop-size distribution, drag coefficients, droplet interference effects, and the effects of chemical reaction in the boundary layer are some of the more important of these problems.

University of Wisconsin,
Madison, Wis., May 9, 1957.

APPENDIX A

OTHER METHODS OF CALCULATION

A flow diagram of the IBM 650 program is given in figure 17. Values of T_1 and r for each new time step are extrapolated from the three prior points. The program automatically recycles each step until the assumed and calculated values agree to within a set difference.

A procedure involving the same calculation technique used in the IBM program but utilizing nomographic aids and graphs was devised. Because the stepwise procedure was retained, it was estimated that at best this procedure would require 0.7 hour of errorless calculation per history. Such a procedure offered little advantage to the computing machine method and was thus abandoned.

Appendix D presents the equations used in the calculations. The extreme nonlinearity and complicated coupling of these equations prohibits any hope of an analytical solution for the most general case. The following two important special cases do allow solution.

Steady-State Heat Transfer, $dT_L/d\theta = 0$

In this case equation (D1) can be integrated to give

$$\theta'_t = \int_0^{\theta'_t} d\theta = \left(\frac{r_{0,w}^2}{K}\right)\left(X \int_0^1 \frac{s\ ds}{X + s^{1/2}}\right) = \frac{r_{0,w}^2 F(X)}{K} \qquad (A1)$$

where

θ'_t total lifetime at steady-state condition

$r_{0,w}$ initial radius at steady-state condition

$$K = \frac{D_v P_T}{R_f T_m \rho_l} \ln\left(\frac{P_T}{P_T - P_{f,L}}\right)$$

$$X = \frac{2}{Nu' - 2} = \frac{1}{0.3\ Re^{1/2} Sc^{1/3}}$$

$$F(X) = X \int_0^1 \frac{s\ ds}{X + s^{1/2}}$$

(See list of symbols for undefined quantities.) A closed-form solution of the integral F is given in reference 2, which also gives two limiting values for F. Only the limiting value for large values of X is appropriate to jet engine conditions. In that case F approaches the constant value 0.500. Graphs of g, F, and K for n-decane at 1 atmosphere pressure are given in figures 8 and 9. These graphs can be used in conjunction with a slide rule or desk calculator to obtain θ_t'. A nomographic solution of equation (A1) is also presented in figure 10.

Negligible Mass Transfer, $dm/d\theta = 0$

For this case equation (D1) becomes

$$\frac{dT_L}{d\theta} = \frac{3}{2}\frac{K_m(T_B - T_L)}{r^2\rho_L C_{p,L}}\left(2 + 0.6\ Pr^{1/3}Re^{1/2}\right) \tag{A2a}$$

The equation is applicable to n-decane for liquid temperatures below 550° R. For a range in liquid temperature from 460° to 550° R, the change in radius of a n-decane droplet due to thermal expansion is less than 3.5 percent. Rearranging the equation gives

$$d\theta = \frac{r^2}{C + D(rV)^{1/2}}\frac{dT_L}{T_B - T_L} \tag{A2b}$$

where

$$C = 3K_a/\rho_L C_{p,L}$$

$$D = 0.9K_a\left(\frac{2\rho_a}{\mu_a}\right)^{1/2}\left(\frac{C_{p,a}\mu_a}{K_a}\right)^{1/3}\Bigg/ C_{p,L}\rho_L$$

The properties of air are evaluated at the mean temperature,

$$T_m = \frac{2T_B + T_{L,0} + 550}{4}$$

A tabulation of C and D (see table I) for n-decane shows that these factors change only slightly over a 50° R range in T_m. Thus, integrating gives

$$\theta_t = \frac{r^2}{C + D(rV)^{1/2}}\ln\left(\frac{T_B - T_{L,0}}{T_B - 550}\right) \tag{A2c}$$

While these two special cases are very useful, they do not directly give any information about the important part of the heating period. If the unsteady-state time $\theta_{t,u}$ and the steady-state temperature T_w are known, the following approximation to the temperature history may be made:

$$T^* = \frac{T_L - T_{L,0}}{T_w - T_{L,0}} = \frac{\theta}{\theta_{t,u}} \qquad \text{for} \quad \theta \leq \theta_{t,u}$$

$$T^* = 1 \qquad \text{for} \quad \theta \geq \theta_{t,u}$$

With this approximation it is possible to obtain integrable forms of equation (D1). These forms are, however, highly complicated. A further objection to this method is the required knowledge of $\theta_{t,u}$. Higher order approximations to the temperature histories give unintegrable forms and require the knowledge of an additional temperature-time point.

Various equations were fit to the temperature and mass histories in an attempt to represent these curves with a universal formula. The following equations give reasonable accuracy:

$$T^* = \frac{T_w - T_L}{T_w - T_{L,0}} = e^{-A\theta^n} \tag{A3}$$

$$1 - m^* = \frac{m}{M_0} = \exp\left[B\left(\frac{\theta}{\theta_{t,u}}\right)^m\right] \tag{A4}$$

Values of constants A, B, n, m are needed for very good accuracy. No good correlation of these constants with ambient conditions could be found. This representation further indicated that a reduced plot of some kind was possible. The values of B and m indicated that a reduced plot should be based on a fixed initial liquid temperature.

Another simplified calculation technique is given here for completeness. This method calculates the time to reach steady-state temperature assuming no mass transfer. From this point on, the steady-state vaporization equation is used. The calculation for the unsteady-state time thus ignores the effect of mass transfer on heat transfer, the latent heat of vaporization, and the change in droplet radius. These effects may be large, since 40 to 50 percent of the drop may vaporize during the unsteady state. While the method is approximate, comparisons given in figure 14 show that it is a very definite improvement over the simple steady-state calculations.

APPENDIX B

CONSTRUCTION OF θ_t' NOMOGRAM

The θ_t' nomogram (fig. 10) referred to in the body of the report was constructed from computed values of the functions and the physical properties given in reference 6. The nomogram calculates the value of θ_t' from the equations

$$\theta_t' = \frac{r^2}{K(T_w)} F(X)$$

$$X = (rV)^{1/2} g(T_w)$$ (see p. 18)

The construction with the form suggested in reference 6 is outlined as follows:

(1) $\log (r) + \log (V) = q_1$

(2) $2 \log (X) = q_1 + 2 \log (g)$

(3) $\log (F) + 2 \log (r) = q_2$

(4) $\log (\theta_t') = q_2 - \log (K)$

Variable	Range	Scale modulus	Plotting modulus	Matching point
r	4×10^{-5} to 4×10^{-3}	14	14	4×10^{-5} (bottom base)
V	10 to 10^3	14	14	10 (bottom)
q_1		$\frac{14\times14}{14+14} = 7$		
g	3.563 to 6.000	65	130	3.563 (bottom)
X		$\frac{7\times65}{7+65} = 6.3194$	12.639	7.126×10^{-2} (bottom)
F	0.090 to 0.500	40	40	0.090 (top base)
r	4×10^{-5} to 4×10^{-3}	7	14	4×10^{-5} (top)
q_2		$\frac{7\times40}{7+40} = 5.957$		
K	10^{-5} to 8.0816×10^{-5}	32	-32	8.0816×10^{-5} (top)
θ_t'		$\frac{5.96\times32}{5.96+32} = 5.022$	5.022	1.78×10^{-6} (top)

Distances between scales:

$\overline{r_1 V}$	arbitrary 10"
$\overline{q_1 r_1}$	$\frac{14}{28}$ 10 = 5"
$\overline{q_1 g}$	arbitrary 12"
$\overline{q_1 X}$	$\frac{7}{7+65}$ 12 = 1.167"
$\overline{Fr_2}$	arbitrary 6.7"
$\overline{q_2 F}$	$\frac{40}{47}$ 6.7 = 14"
$\overline{q_2 K}$	arbitrary 14"
$q_2 \theta'_t$	$\frac{5.96}{5.96+32}$ 14 = 2.198"

Since there are actually two nomograms connected through the function $F(X)$, the distance between the F and X scales is purely arbitrary and does not affect the other scale distances.

The scales from left to right as they appear on the nomogram are: r_1, q_1, s, F, V, q_2, r_2, θ'_t, g, K.

Scale construction: The F and X scales were matched from IBM 650 computed values of F against s. The scales g, K, X, F were specially computed for each scale division. The scales r, V, and θ'_t were taken from logarithmic scales provided in reference 6. The scales g and K were marked in terms of the independent variable T_w.

Calculation proceeds as follows:

(1) Pick the values of $r_1 = r_2$, V, and T_w of interest.

(2) Draw a line from r_1 to V.

(3) From the intersection of $r_1 V$ on q_1, draw a line to $g(T_w)$.

(4) Read the value of X at the intersection of $q_1 g$ on X.

(5) Find the point on the F scale that equals this value of X.

(6) Draw a line from F to r_2.

(7) From the intersection of this Fr_2 line with q_2 draw a line to $K(T_w)$.

(8) The intersection of this q_2K line with the θ_t' scale gives the desired value of θ_t'.

Construction of such a nomogram requires many hours of tedious work. It is therefore felt that if values of θ_t' are desired for other fuels, the graphs of F, g, and K should be drawn and used directly. A nomogram should be constructed only in cases where very extensive use is anticipated.

APPENDIX C

EXAMPLE OF CALCULATIONS USING VARIABLE VELOCITY AND CHARTS OF REDUCED VARIABLES

As an example of the method of reduced-variable charts, the following initial conditions will be used:

Air temperature, T_B, $^\circ R$	1380
Initial relative air velocity, $V_{a,0}$, in./sec	1000
Initial radius, r_0, in.	0.001
Initial diameter, microns	50
Initial liquid temperature, $T_{L,0}$, $^\circ R$	600

Ingebo's drag coefficient (ref. 5) is used here:

$$C_D = \frac{27}{Re^{0.84}}$$

$$\frac{dV}{d\theta} = -\frac{3}{8}\left(\frac{\rho_a}{\rho_L}\right)\left(\frac{V^2}{r}\right) C_D$$

Step 1: Using only part of the curve of figure 7(a), obtain the reduced curves shown in figure 18. The origin of the new axis is 0.065 on the curve of figure 7(a). Thus, only the θ^* scale must be revised. For example, 15 percent is vaporized at $\theta^* = 0.25$ on the new scale instead of $\theta^* = 0.3$ as on the old scale.

Step 2: Obtain values of θ_t for various velocities. For $\theta^* = 0.8$, $T_w = 736$, $m^* = 0.9$ calculate $r_w^* = 0.475$, $r_w = 0.000475$; $\theta_t = \theta_t'/0.2 = 5\theta_t'$. Thus, $\theta_t \times 10^3 = 4.42$, 4.62, 4.75, and 4.88 seconds; $V = 1000$, 900, 800, and 700 inches per second. Plot these values as in figure 18.

Step 3: Pick $\Delta\theta = 5\times10^{-4}$.

Step 4: Calculate the velocity at time $\Delta\theta$ by using the drag equations:

$$V_1 - V_2 = \frac{3}{4}\frac{\rho_a}{\bar{r}^{1.84}}\frac{\bar{V}_a^{0.84}}{\bar{P}_L}\bar{V}^{1.16}\Delta\theta = K\,\Delta\theta\bar{V}^{1.16}$$

where

$V_1 = 1000$; V_2 is the velocity at time $\Delta\theta$; $\bar{V} = (V_1 + V_2)/2$

$\rho_a(1380) = 1.66\times10^{-5}$

$\bar{r} = 0.001$

$\rho_L(625) = 0.02487$ (estimating $\Delta\theta^*$ will be ≈ 0.1)

$V_a \frac{T_B + \bar{T}_L}{2} = V_a(1000) = 0.0646$

5080

For a starting value, use $V_2 = \frac{V_1}{1 + \frac{K\Delta\theta}{2}}$. After this, extrapolation of the velocity curve should be used to obtain V_m.

$$K = \frac{3\times1.66\times10^{-5}(0.0646)^{-0.84}}{2.487\times10^{-2}}$$

$K = 16.6$

CA-4

$\bar{V} = 990$

$V_2 = V_1 - 16.6(3000)(5\times10^{-4}) = 1000 - 25 = 975$

Recalculate $\bar{V} = \frac{V_1 + V_2}{2} = 988.$

Step 5: $\theta_{t,1} = 4.47$ from the graph of step 2.

Step 6: $\Delta\theta^*_1 = \frac{\Delta\theta}{\theta_{t,1}} = \frac{5\times10^{-4}}{4.47\times10^{-3}} = 0.113$; $\theta^*_1 = 0.113$

Step 7: The first point of the m^*, θ curve is $(0.025, 5\times10^{-4})$.

Step 8: The guesses of r_0 and T_1 were very close to the calculated values, and thus no recalculation is necessary. Repeat, beginning with step 4, to find the second point of the m^*, θ curve.

$V_2 = 975$; $V_3 = ?$

$\rho_a(1380) = 1.66\times10^{-5}$

$\bar{r} = 0.0096$ (examine r^* graph; assume $\Delta\theta^* = 0.1$)

$\rho_L(680) = 0.02397$

$V_a(1030) = 0.0686$

$\overline{V} = 963$ (linear extrapolation of previously calculated points)

$$K = \frac{7.5 \times 1.66 \times (68.6)^{0.84} 10^{-1}}{0.93 \times 2.397} = 19.6$$

$V_3 = 975 - 29.4 = 946$

$\theta_{t,2} = 4.53 \times 10^{-3}$

$$\Delta\theta_2^* = \frac{5 \times 10^{-4}}{4.53 \times 10^{-3}} = 0.110; \quad \theta_2^* = 0.223$$

The second point of the m^*, θ curve is $(0.125, 10^{-3})$. The guess of $\overline{T}_L$ was quite good; $\overline{r}$ was close enough. Clearly on the next step $\overline{r}$ will be approximately 0.00094, and so forth. Repeat to obtain third point, and so forth.

5080

APPENDIX D

RESUMÉ OF EQUATIONS USED IN CALCULATIONS

The following equations were used in the calculations of histories; they are derived and discussed in references 1 and 2. They are repeated here for convenient reference:

$$\frac{dm}{d\theta} = \left(\frac{-2\pi r D_v P_T}{R_f T_m}\right)\left(\ln \frac{P_T}{P_T - P_{f,L}}\right)\left[2 + 0.6\left(\frac{2rV\rho_m}{\mu_m}\right)^{1/2}\left(\frac{\mu_m}{\rho_m D_v}\right)^{1/3}\right] \quad (D1)$$

$$\frac{dT_L}{d\theta} = \left[\frac{2\pi r K_m (T_B - T_L)}{mC_{p,f}}\right]\left(\frac{z}{e^z - 1}\right)\left[2 + 0.6\left(\frac{2rV\rho_m}{\mu_m}\right)^{1/2}\left(\frac{C_{p,m}\mu_m}{K_m}\right)^{1/3}\right] - \left(\frac{\lambda}{mC_{p,L}}\frac{dm}{d\theta}\right) \quad (D2)$$

where

$$m = 4/3(\pi r^3 \rho_L)$$

$$\frac{dm}{d\theta} = 4\pi r^2 \rho_L \frac{dr}{d\theta} + \frac{4}{3}\pi r^3 \frac{d\rho_L}{d\theta}$$

$$T_m = \frac{T_B + T_L}{2}$$

$$z = \frac{C_{p,f}\frac{dm}{d\theta}}{2\pi r K_m\left[2 + 0.6\left(\frac{2rV\rho_m}{\mu_m}\right)^{1/2}\left(\frac{C_{p,m}\mu_m}{K_m}\right)^{1/3}\right]}$$

$$\overline{M} = \left(1 - \frac{P_{f,L}}{2P_T}\right)M_a + \left(\frac{P_{f,L}}{2P_T}\right)M_f$$

$$\rho_m = \frac{P_T \overline{M}}{R T_m}$$

$$\mu_m = \left(1 - \frac{P_{f,L}}{2P_T}\right)\mu_a + \left(\frac{P_{f,L}}{2P_T}\right)\mu_f$$

$$K_m = \left(1 - \frac{P_{f,L}}{2P_T}\right) K_a + \left(\frac{P_{f,L}}{2P_T}\right) K_f$$

$$C_{p,m} = \left(1 - \frac{P_{f,L}}{2P_T}\right)\left(\frac{M_a}{\overline{M}}\right) C_{p,a} + \left(\frac{P_{f,L}}{2P_T}\right)\left(\frac{M_f}{\overline{M}}\right) C_{p,f}$$

D_v, μ_a, μ_f, K_a, K_f, $C_{p,a}$, and $C_{p,f}$ are taken at temperature T_m. $P_{f,L}$, ρ_L, $C_{p,L}$, and λ are taken at the liquid temperature T_L, which is assumed uniform throughout the drop (ref. 2). The equations for the physical properties may be found in reference 7.

5080

REFERENCES

1. El Wakil, M. M., Uyehara, O. A., and Myers, P. S.: A Theoretical Investigation of the Heating-Up Period of Injected Fuel Droplets Vaporizing in Air. NACA TN 3179, 1954.

2. El Wakil, M. M., Priem, R. J., Brikowski, H. J., Myers, P. S., and Uyehara, O. A.: Experimental and Calculated Temperature and Mass Histories of Vaporizing Fuel Drops. NACA TN 3490, 1956.

3. Priem, R. J., Borman, G. L., El Wakil, M. M. Uyehara, O. A., and Myers, P. S.: Experimental and Calculated Histories of Vaporizing Fuel Drops. NACA TN 3988, 1957.

4. El Wakil, M. M., Myers, P. S., and Uyehara, O. A.: Fuel Vaporization and Ignition Lag in Diesel Combustion. SAE Trans., vol. 64, 1956, pp. 712-726; discussion, pp. 726-729.

5. Ingebo, Robert D.: Drag Coefficients for Droplets and Solid Spheres in Clouds Accelerating in Airstreams. NACA TN 3762, 1956.

6. Johnson, Lee H.: Nomography and Empirical Equations. John Wiley & Sons, Inc., 1952.

7. Priem, Richard Jerome: Vaporization of Fuel Drops Including the Heating-Up Period. Ph.D. Thesis, Univ. Wis., 1955.

5080

TABLE I. - VALUES OF C AND D PARAMETERS

$$\left[T_m = \frac{2T_B + T_{L,0} + 550}{4};\ \theta_t = \frac{r^2}{C + D(rV)^{1/2}}\right.$$

(See appendix A).]

T_m, °R	C	D
1075	1.378×10^{-4}	1.81×10^{-4}
1050	1.350	1.81
1025	1.320	1.81
1000	1.290	1.81
975	1.260	1.809
950	1.230	1.80
925	1.200	1.788
900	1.170	1.785
875	1.140	1.785
850	1.110	1.785
825	1.080	1.785
800	1.050	1.785
775	1.020	1.785
750	.993	1.785
725	.965	1.785
700	.934	1.785
675	.905	1.785
655	.880	1.785

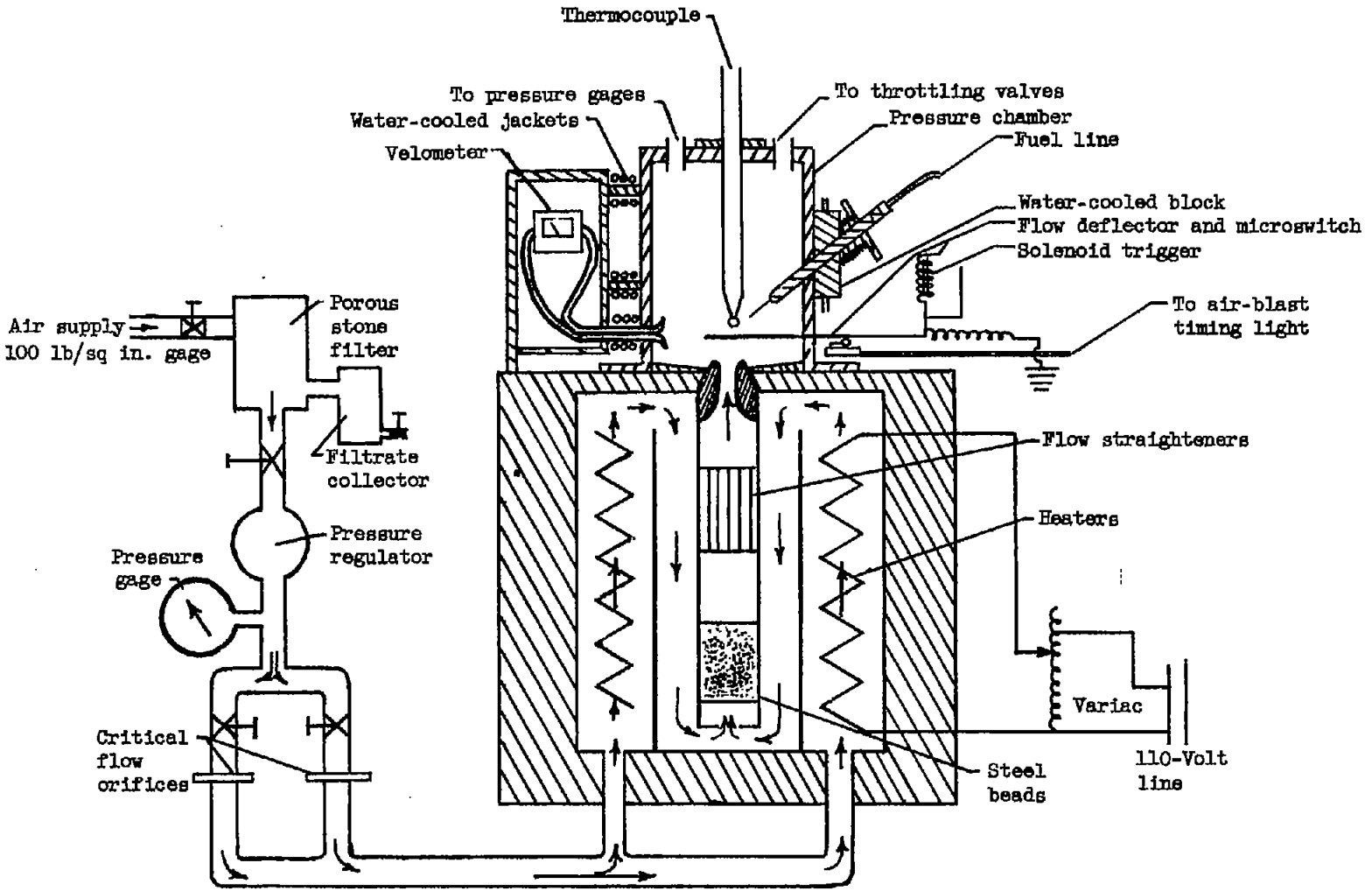

Figure 1. - Experimental apparatus.

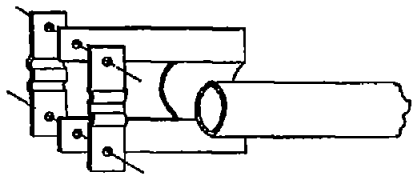

Exploded view of "B"

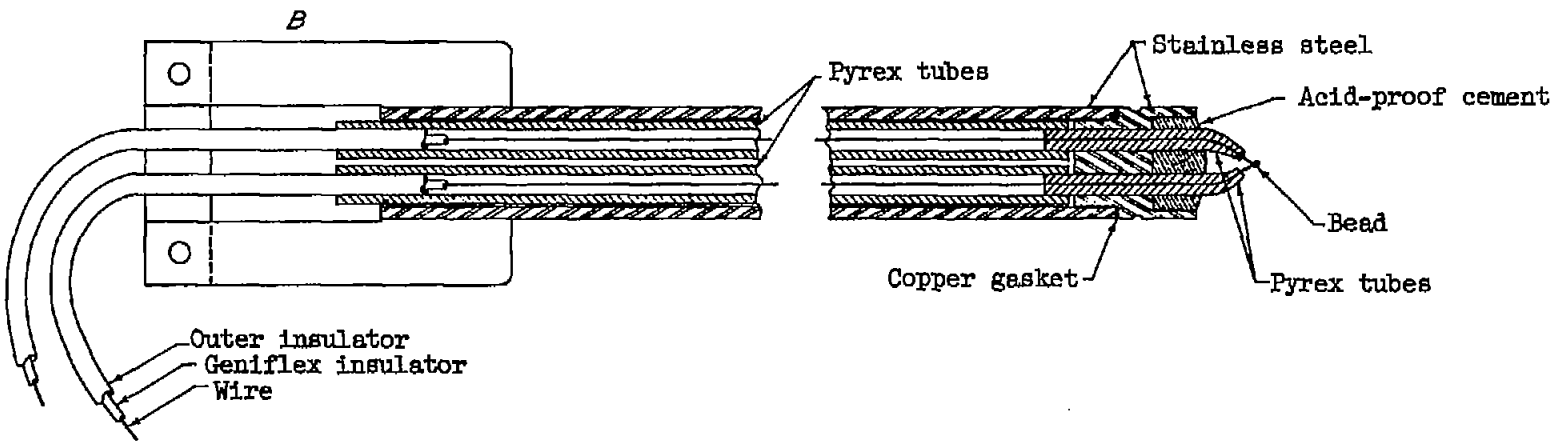

Figure 2. - Thermocouple construction used with pressure data.

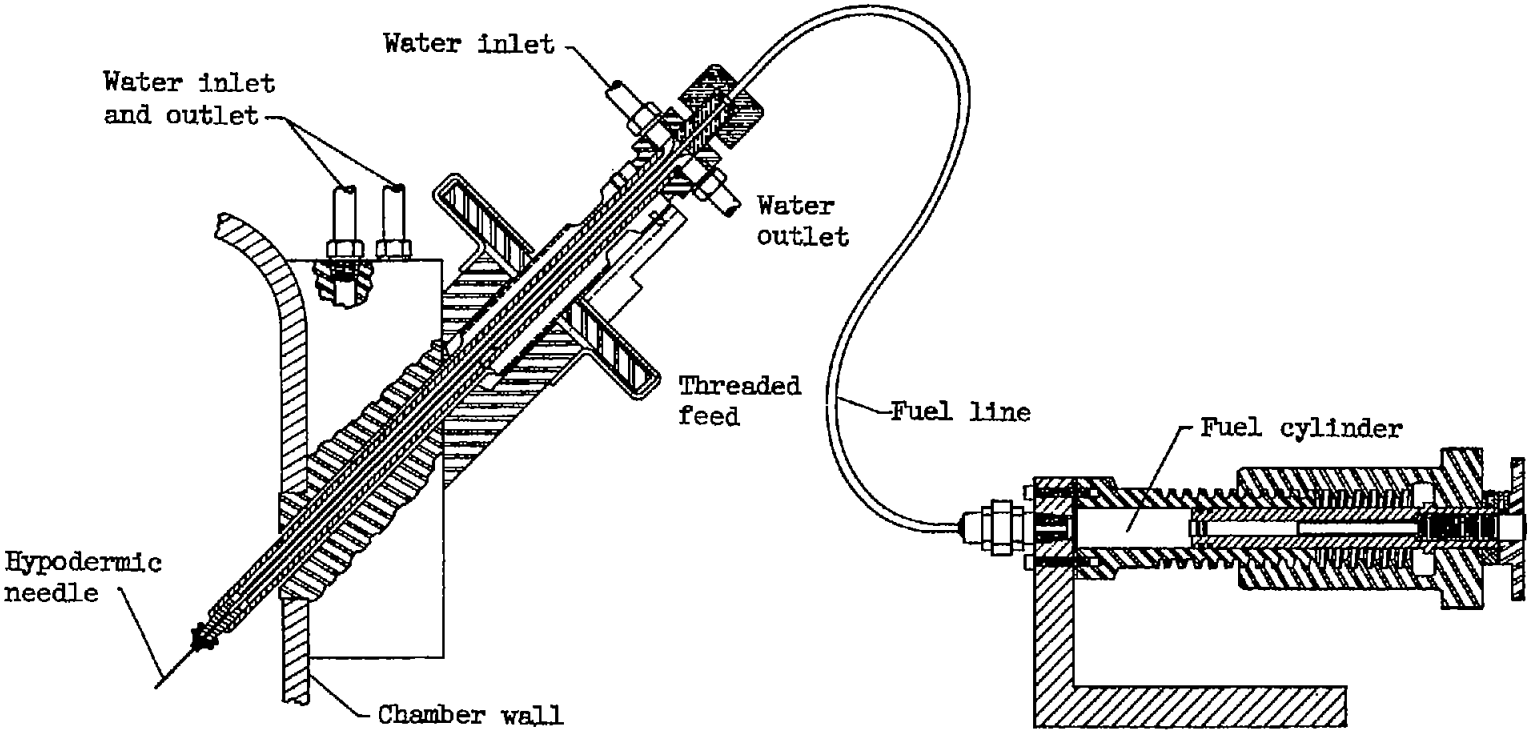

Figure 3. - Fuel handling device.

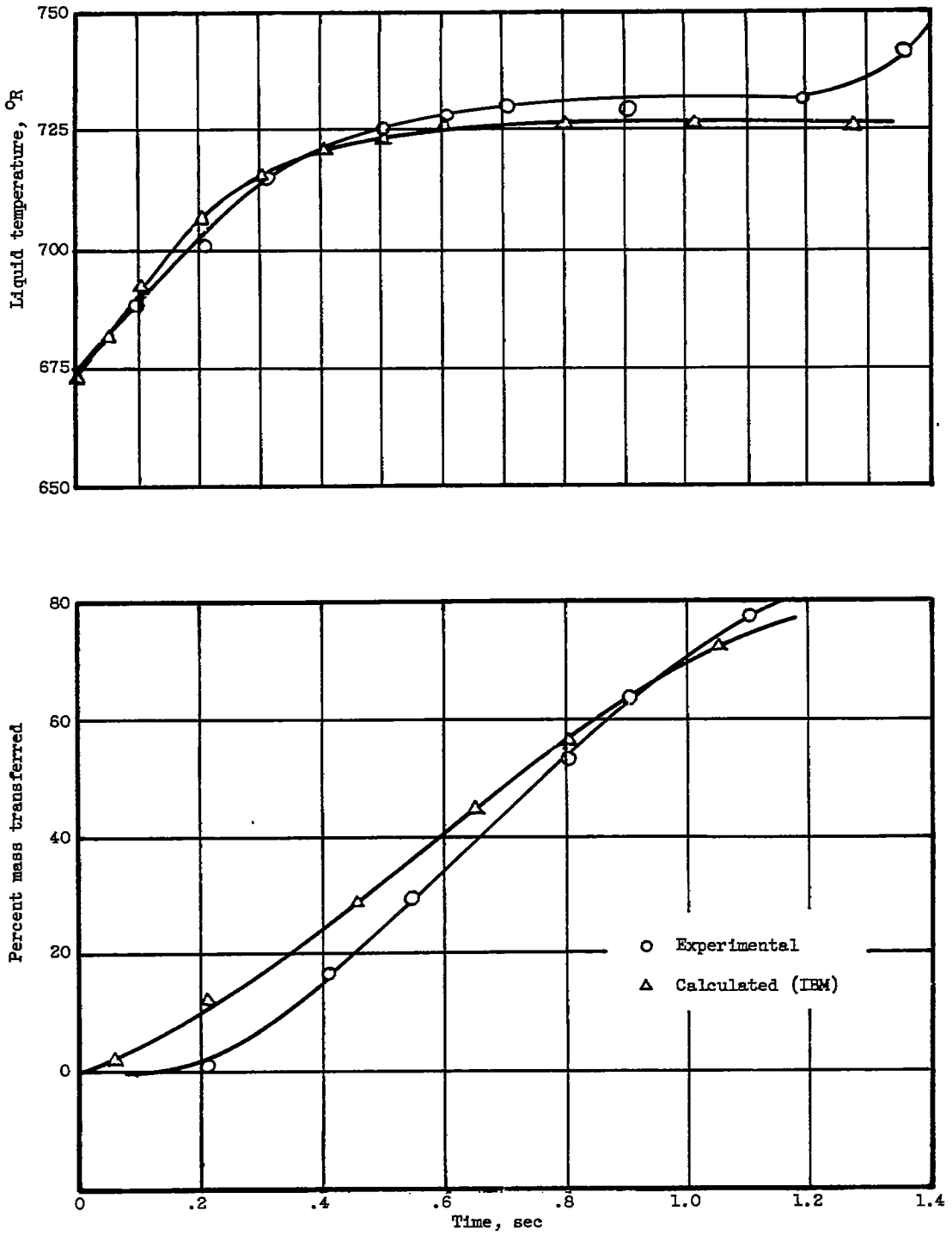

(a) n-Decane; initial diameter, 944 microns.

Figure 4. - Experimental and calculated histories. Total pressure, 2 atmospheres absolute; air temperature, 900° R; air velocity, 130 inches per second.

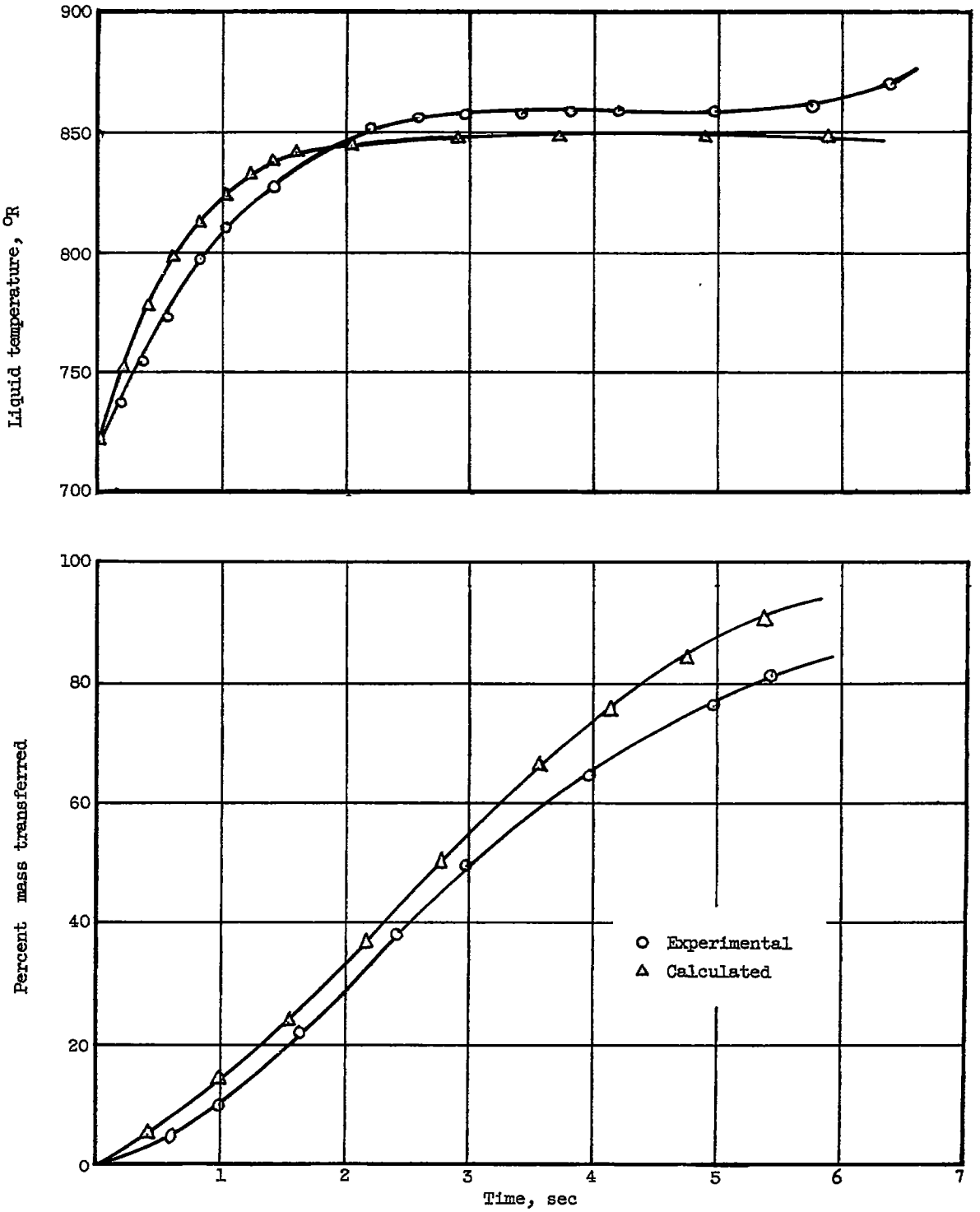

(b) Hexadecane; initial diameter, 1074 microns.

Figure 4. - Concluded.

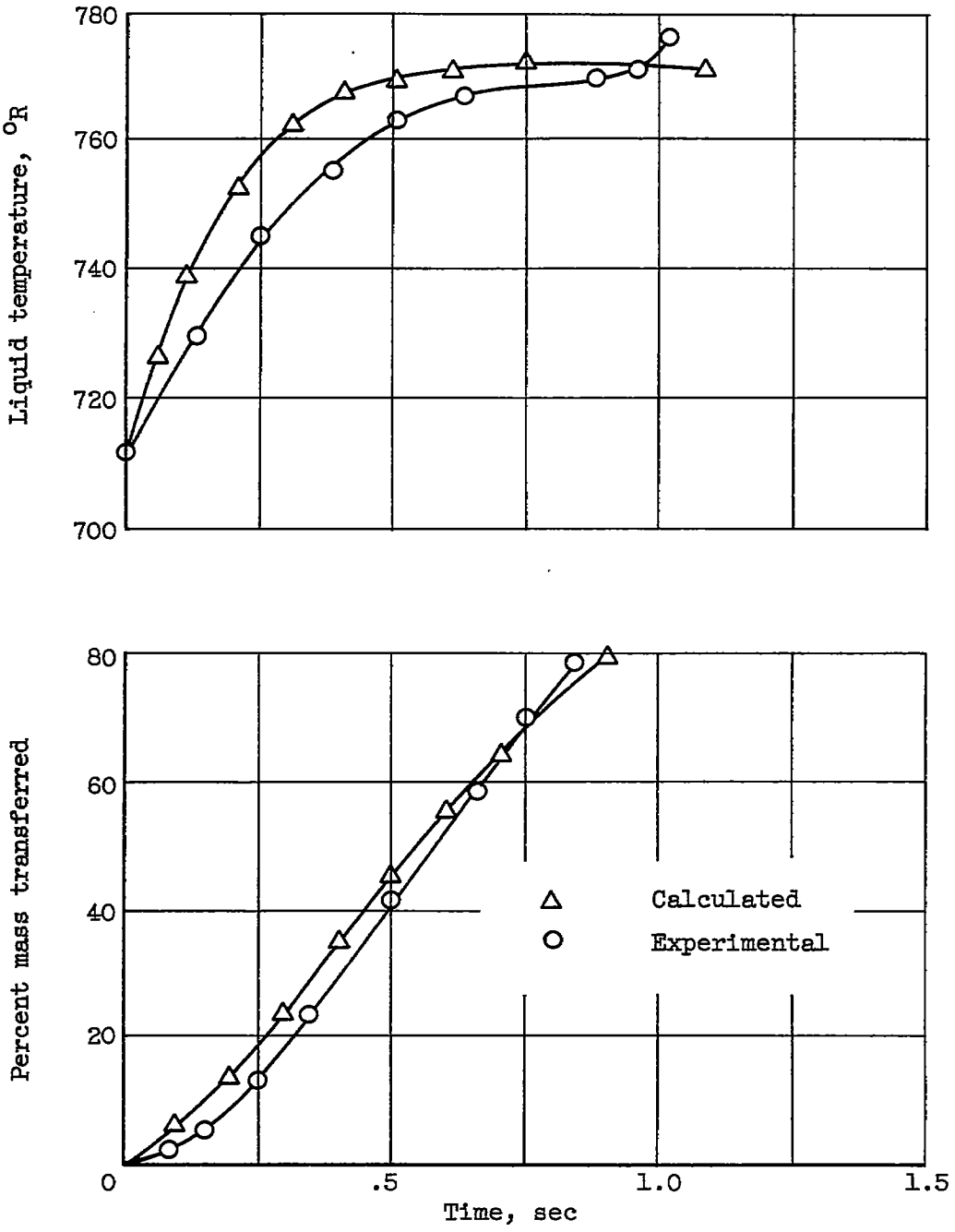

(a) Initial radius, 380 microns.

Figure 5. - Comparison of calculated and experimental histories for n-decane. Total pressure, 4 atmospheres absolute; air temperature, 955° R; air velocity, 45.4 inches per second.

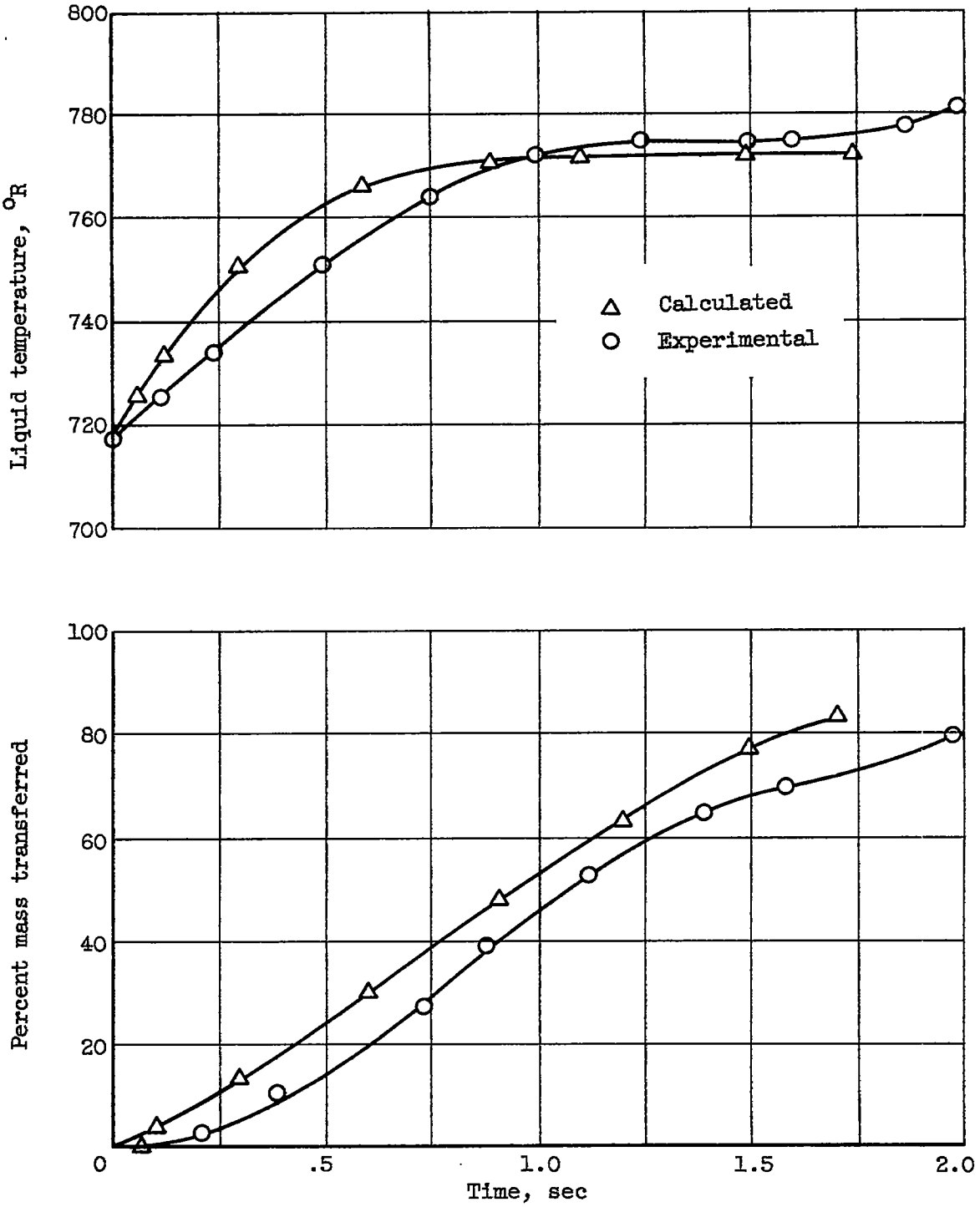

(b) Initial radius, 555 microns.

Figure 5. - Concluded.

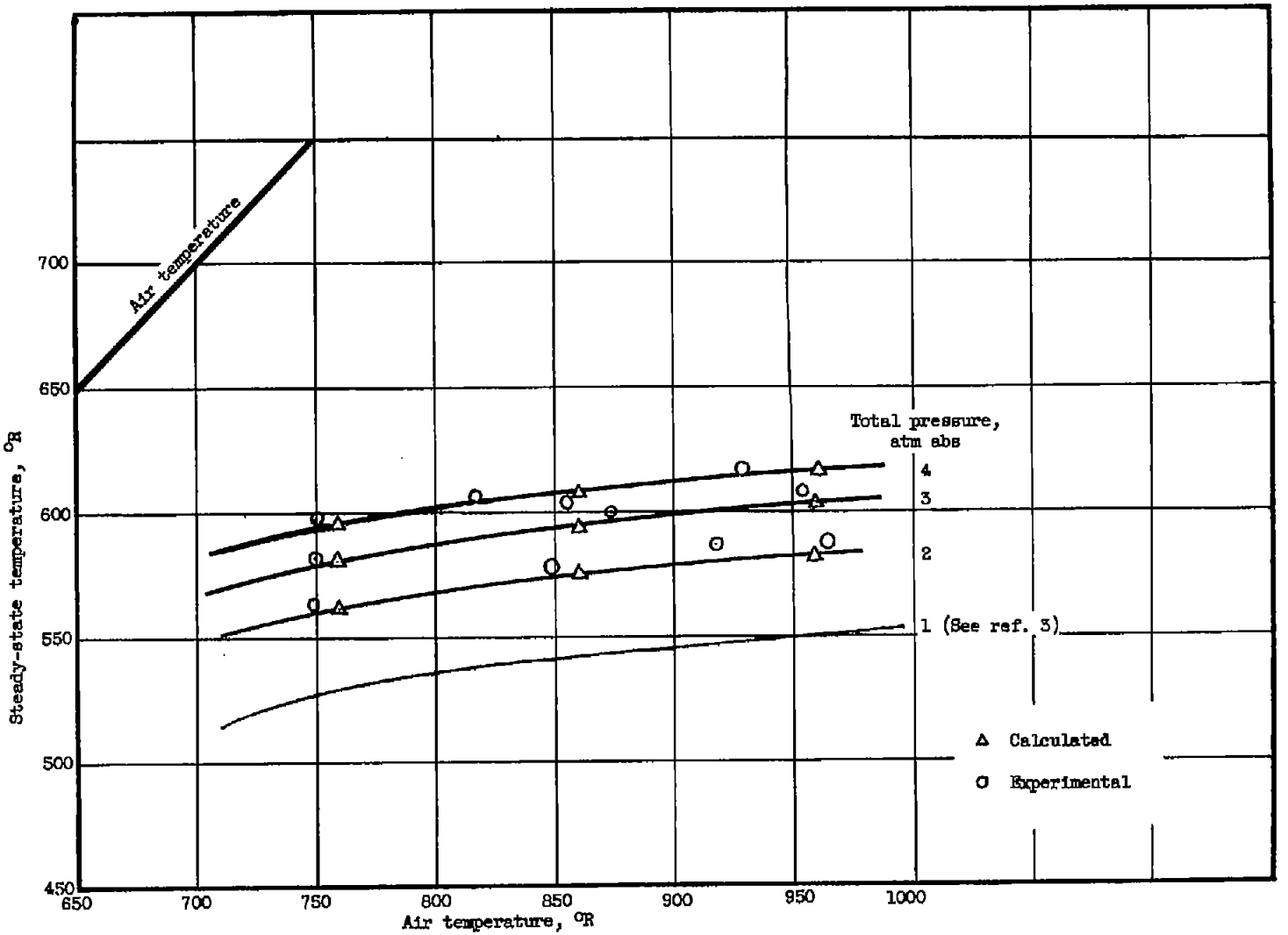

(a) n-Hexane.

Figure 6. - Comparison of calculated and experimental steady-state temperatures at various total pressures.

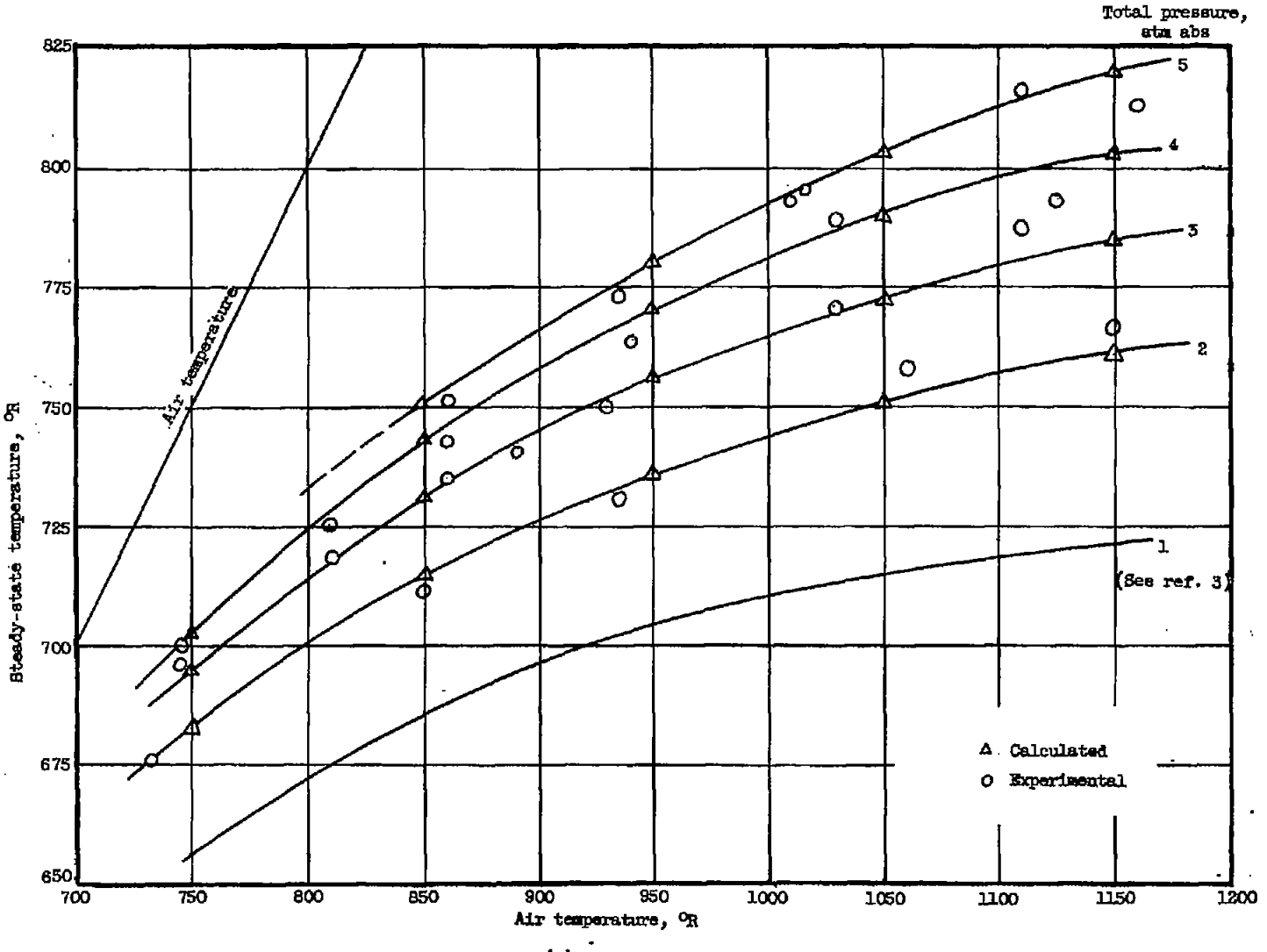

(b) n-Decane.

Figure 6. - Continued.

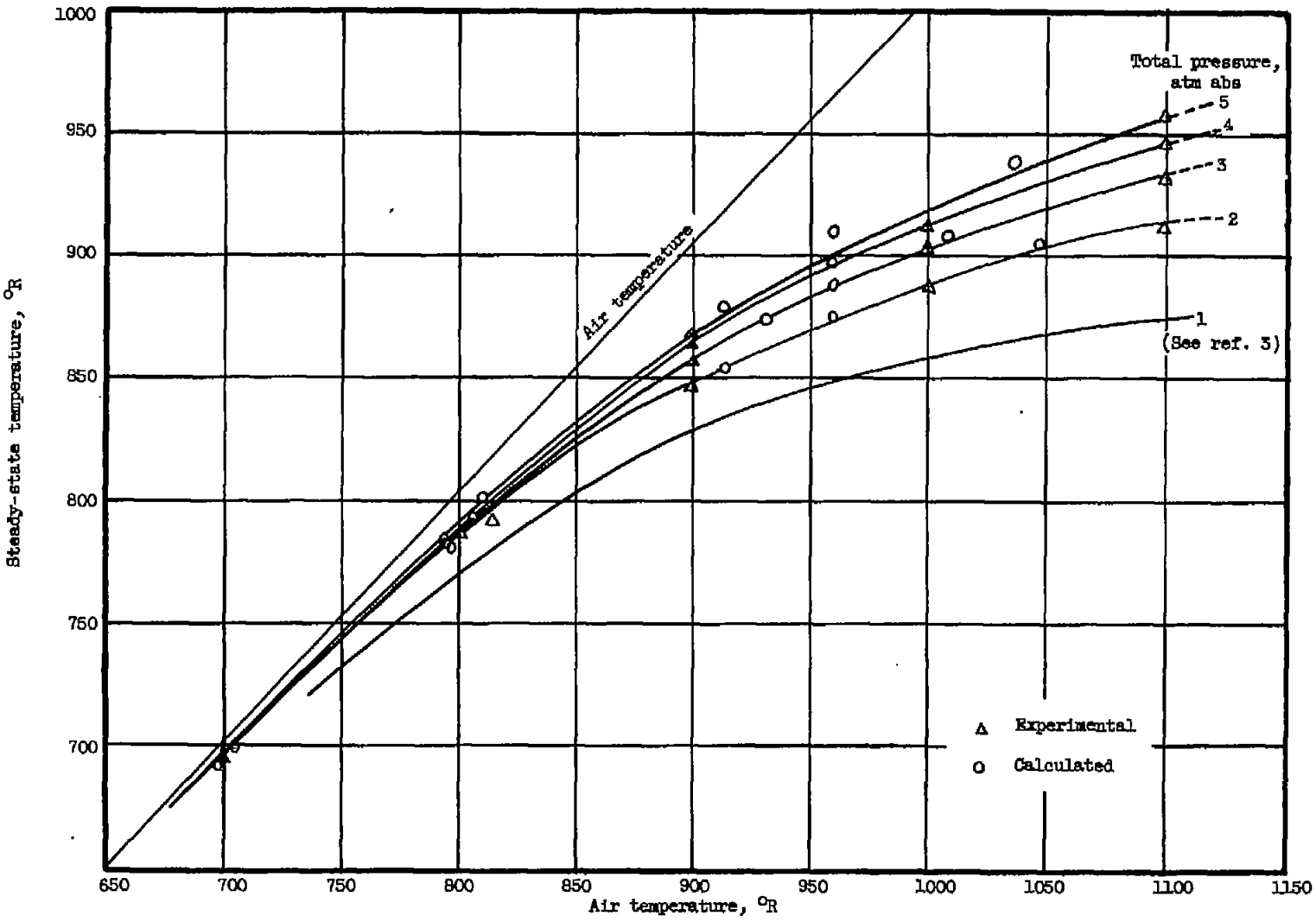

(c) Hexadecane.

Figure 6. - Concluded.

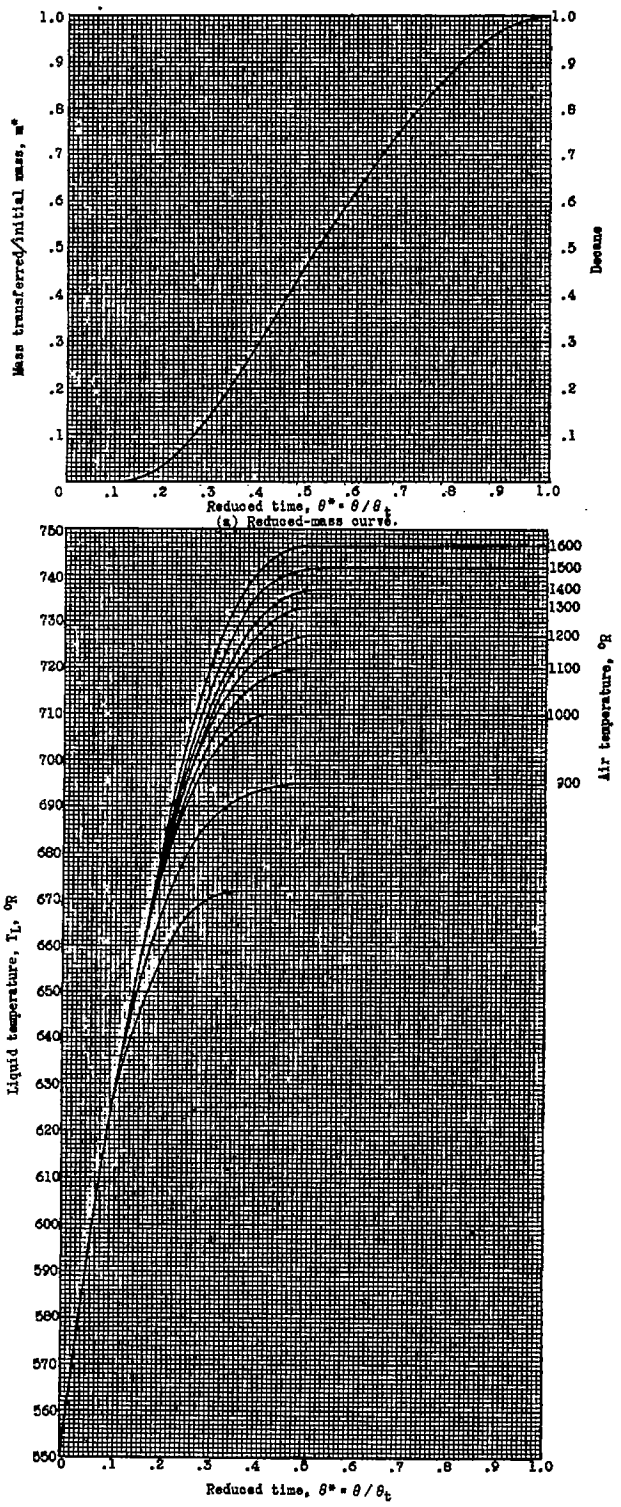

Figure 7. - Reduced mass and temperature curves for n-decane. (A large working copy of this fig. may be obtained by using request card bound in back of report.)

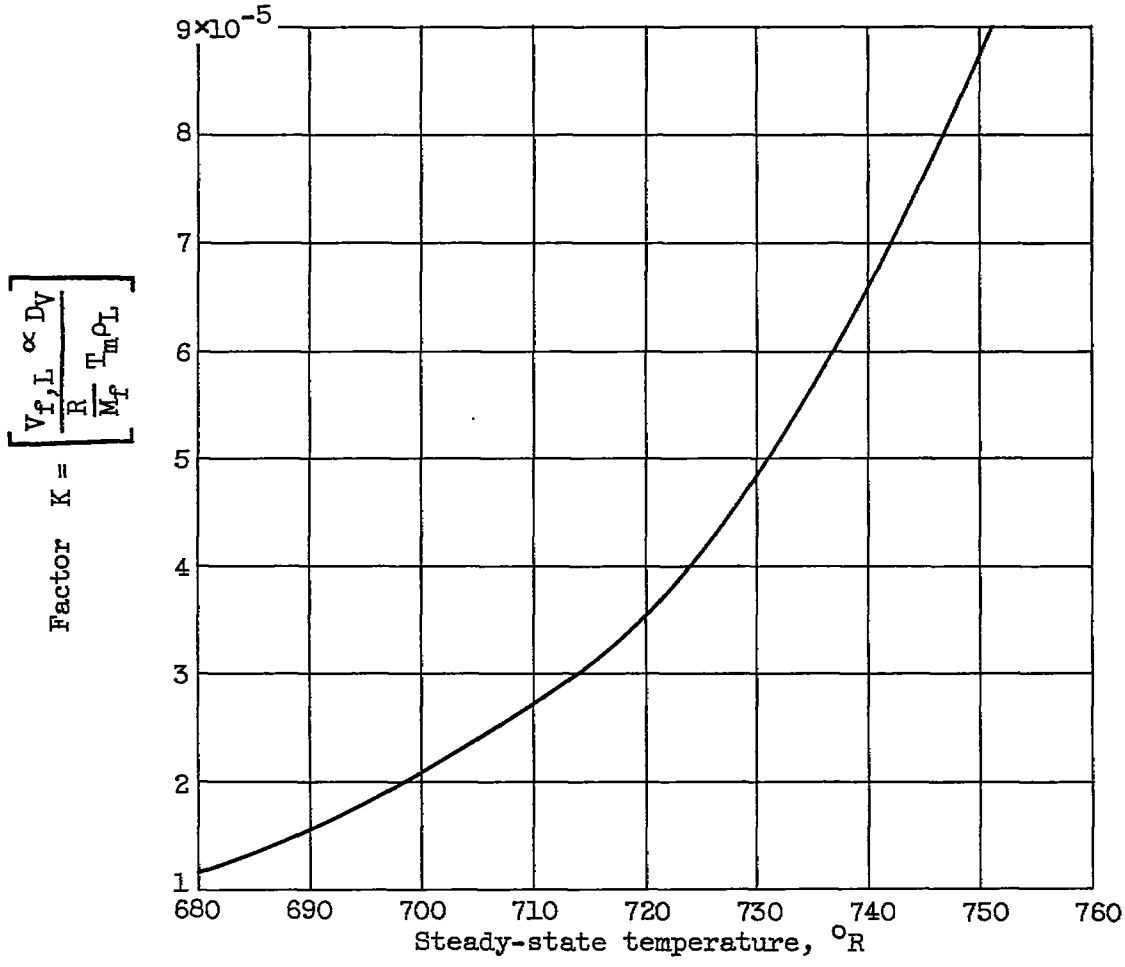

(a) Factor K.

Figure 8. - Various factors plotted against steady-state temperature T_W for calculation of vaporization time. Total pressure, 1 atmosphere.

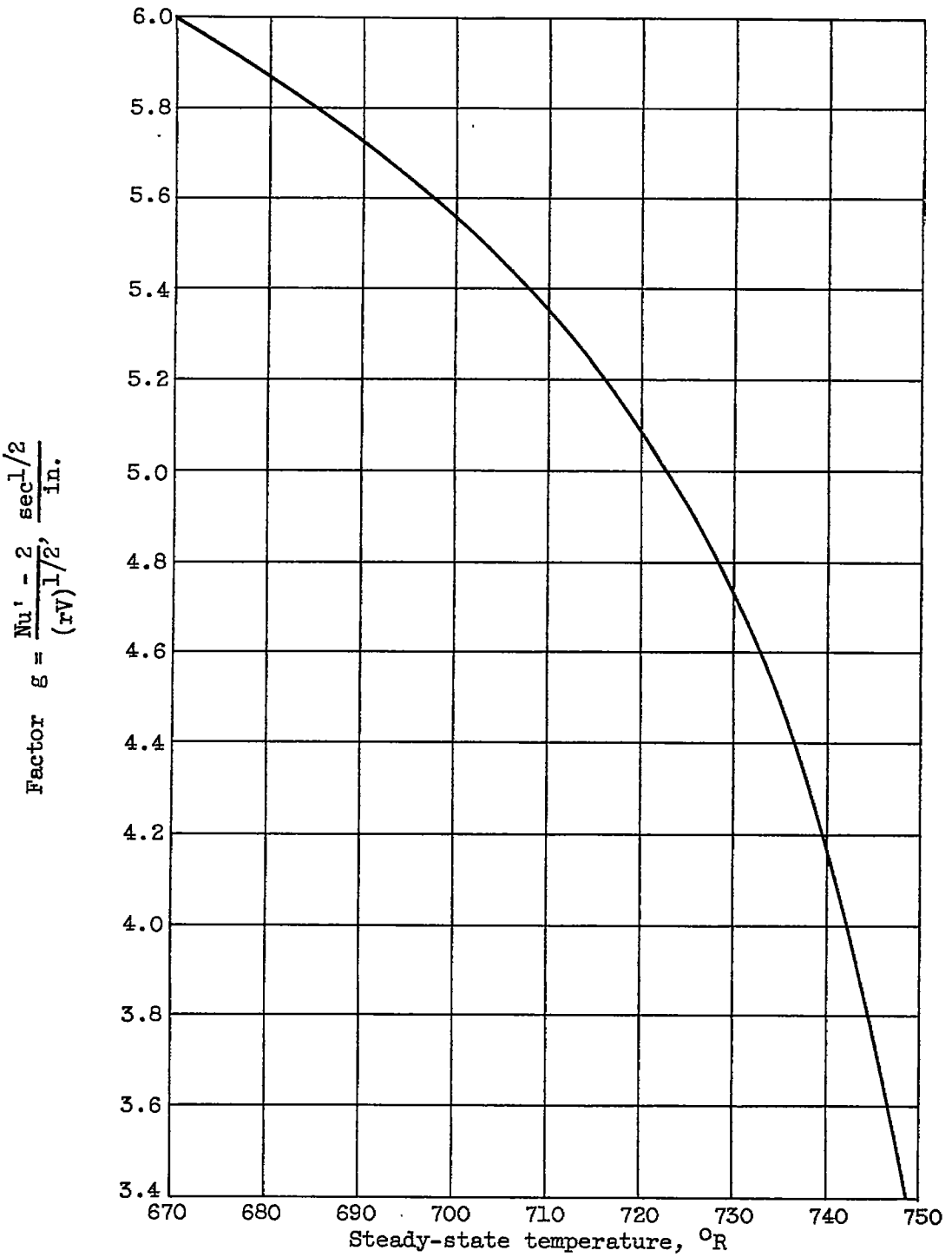

(b) Factor g.

Figure 8. - Concluded.

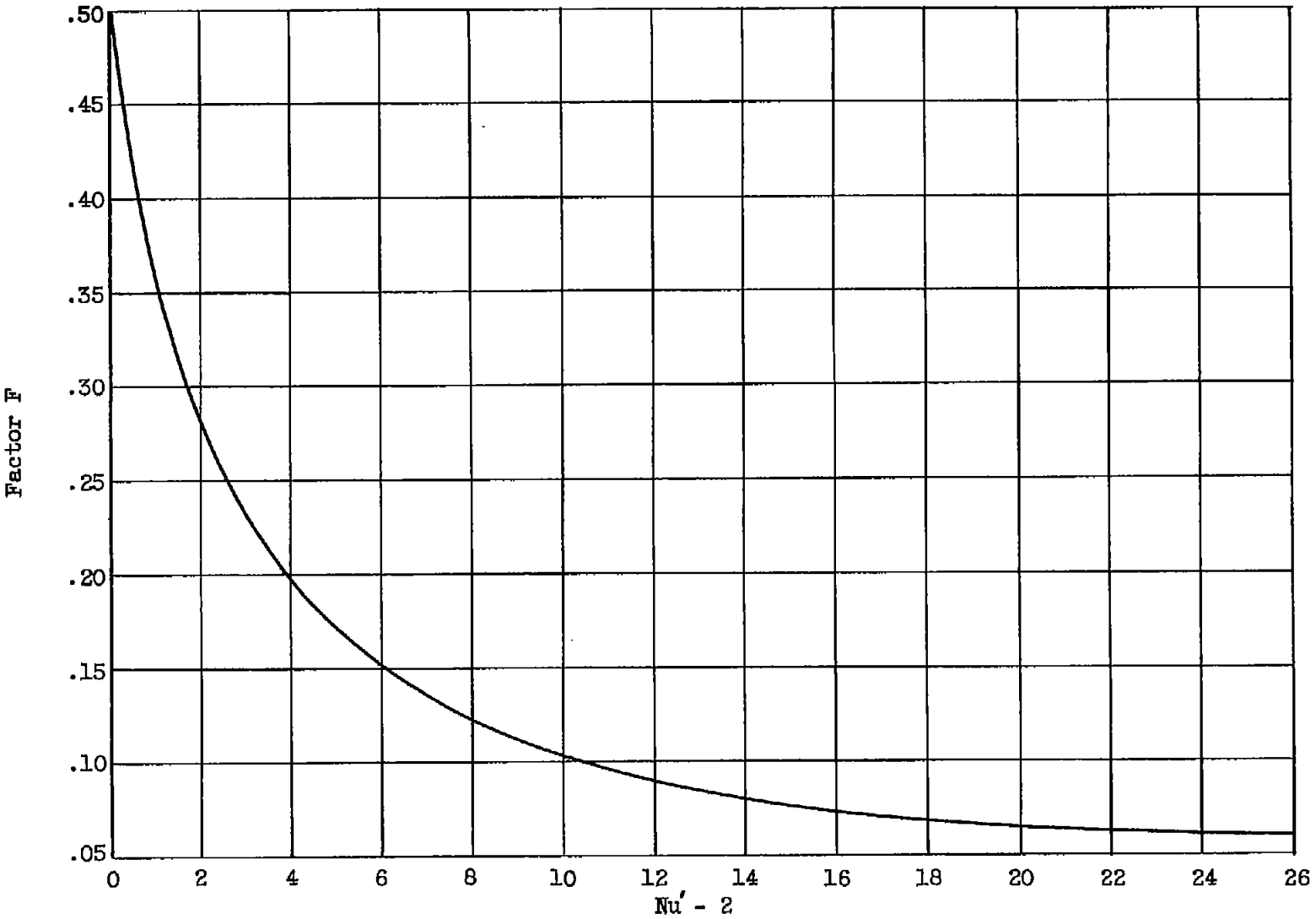

Figure 9. - Factor F plotted against $Nu' - 2$ for calculation of vaporization time at steady-state temperature.

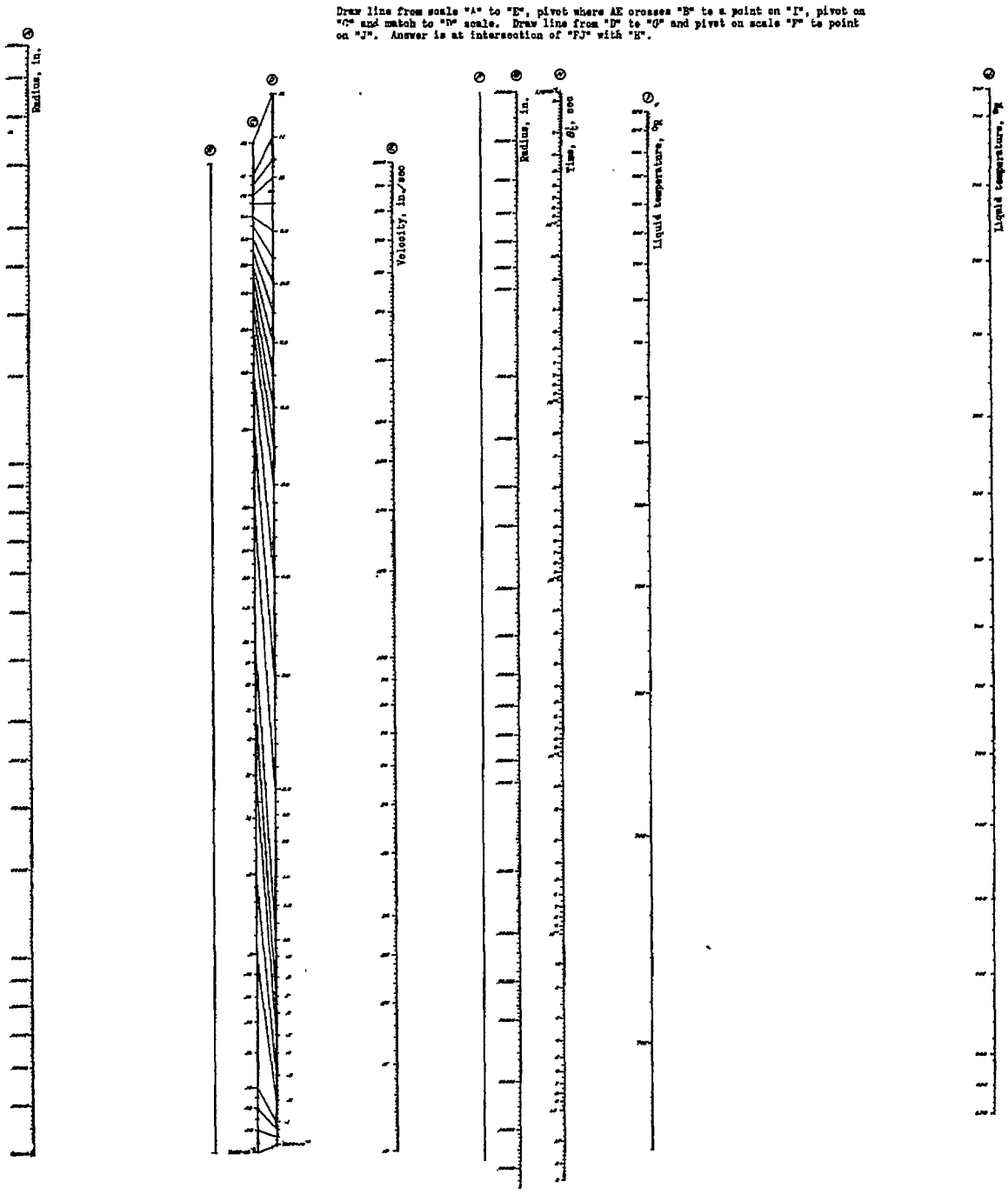

Figure 10. - Nomogram for calculation of θ_t^l. (A large working copy of this fig. may be obtained by using request card bound in back of report.)

5080

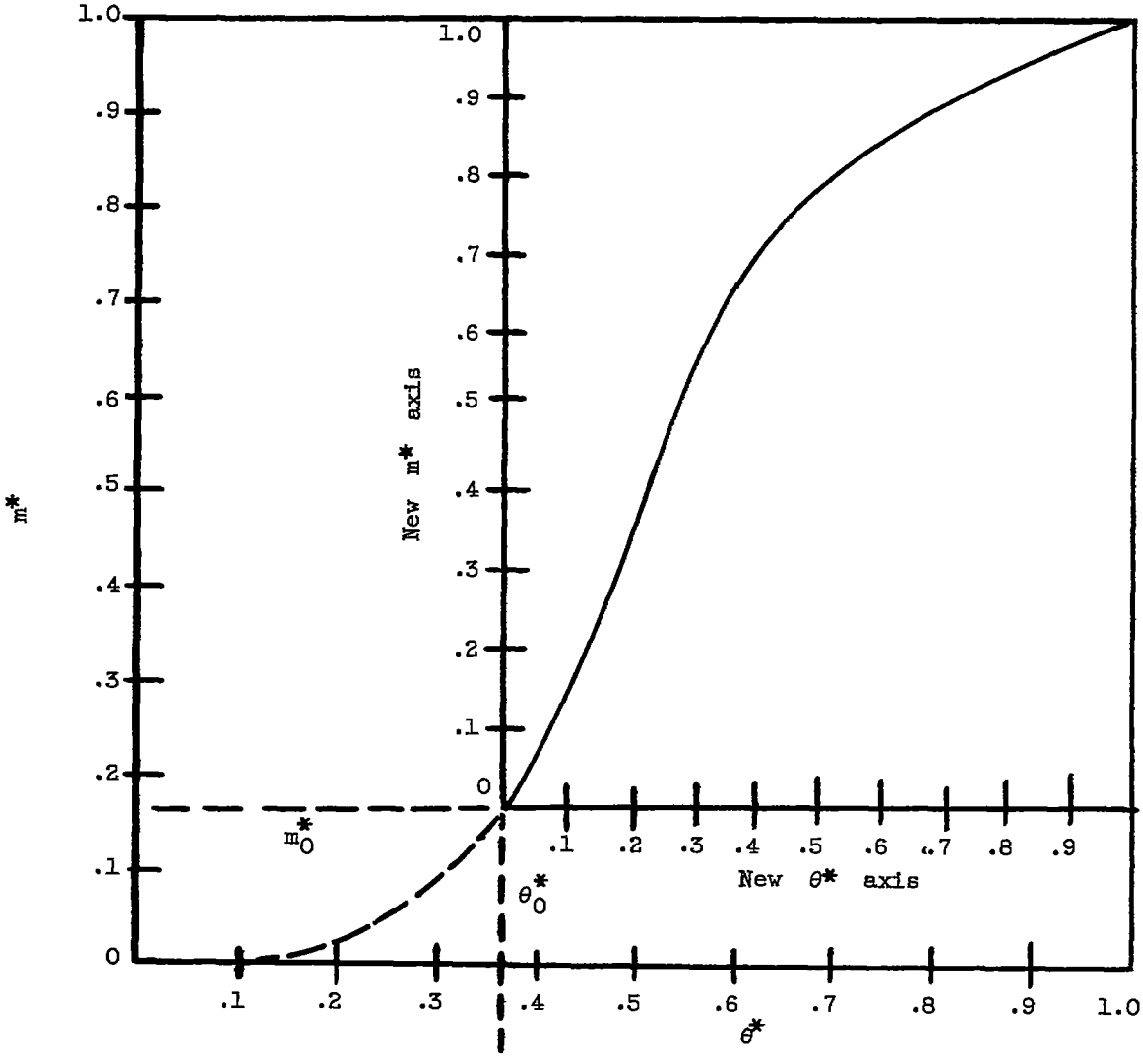

Figure 11. - Construction of new axis; case of initial liquid temperature higher than 550° R for decane. Solid curve and new axis give the desired reduced curve.

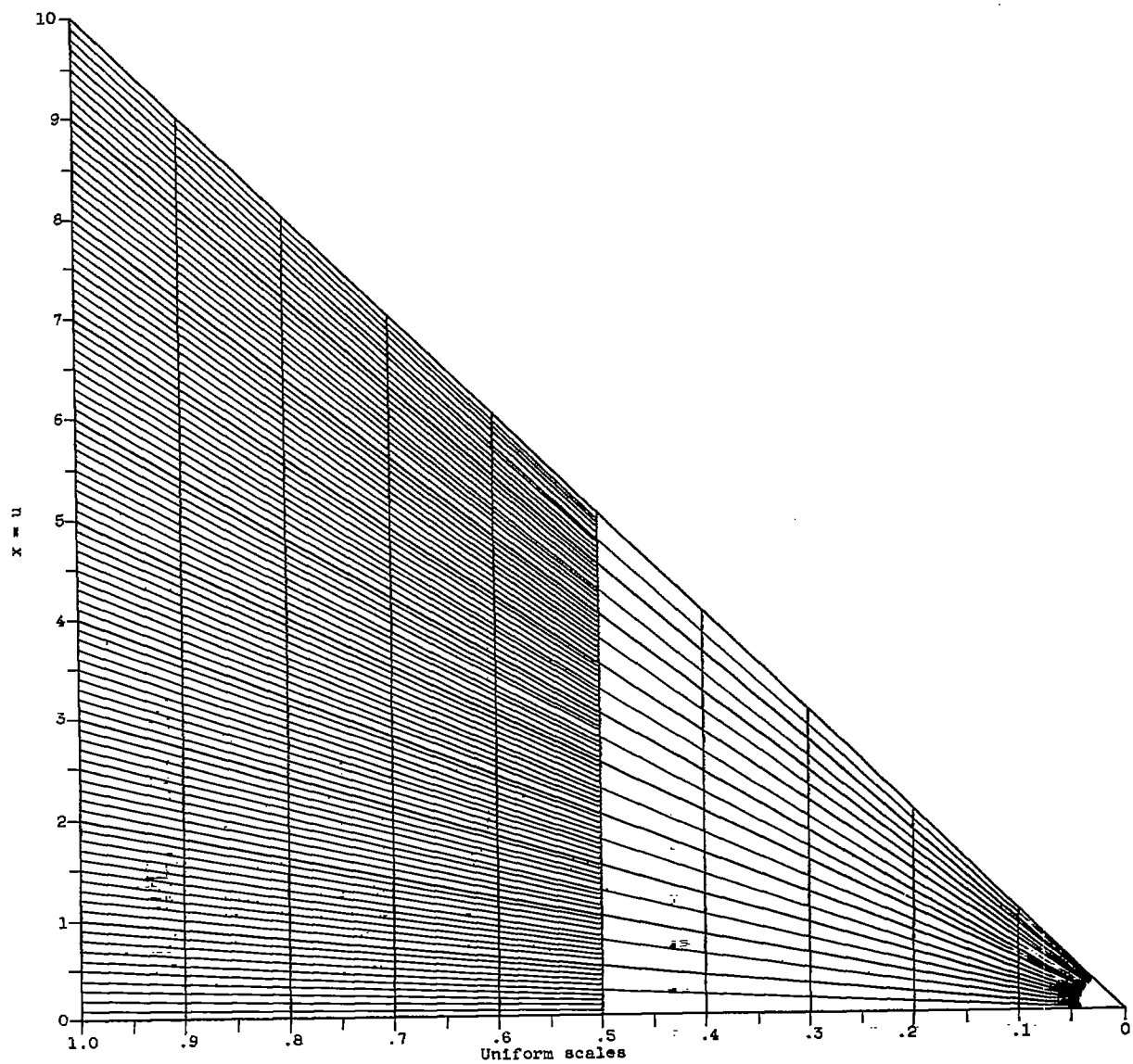

Figure 12. - Uniform scales for construction of scales 10 inches or less in length. (A large working copy of this fig. may be obtained by using request card bound in back of report.)

5080

Draw line from $T_{L(0)}$ scale to $T_{L(\theta)}$ scale. Pivot on intersection with Q and draw line to point on $1-m^*$. Intersection on r^* scale gives corresponding value of r^*.

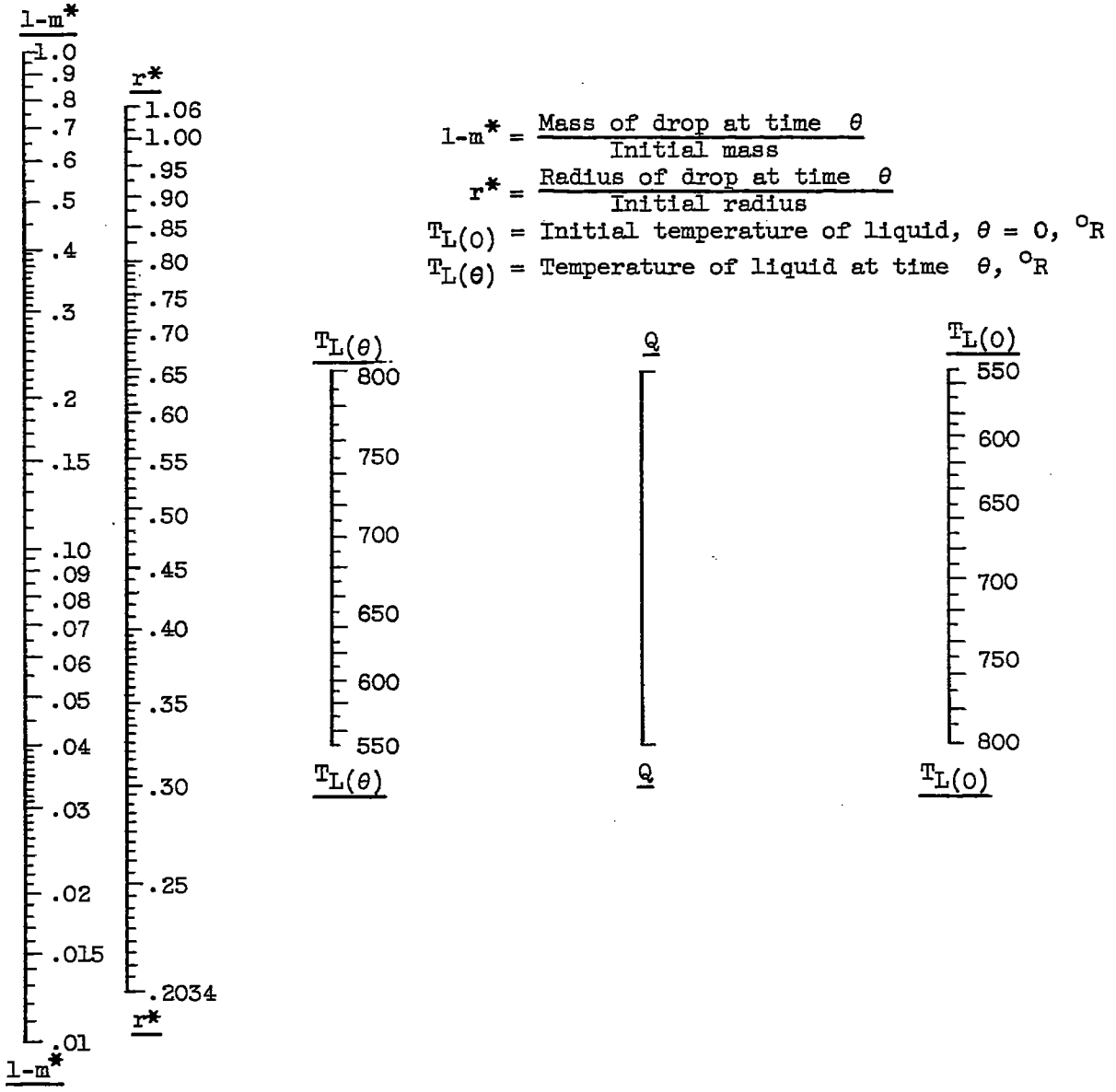

$$1-m^* = \frac{\text{Mass of drop at time } \theta}{\text{Initial mass}}$$

$$r^* = \frac{\text{Radius of drop at time } \theta}{\text{Initial radius}}$$

$T_{L(0)}$ = Initial temperature of liquid, $\theta = 0$, $^\circ R$

$T_{L(\theta)}$ = Temperature of liquid at time θ, $^\circ R$

Figure 13. - Nomogram for calculation of reduced radius from m^*, T_w data.

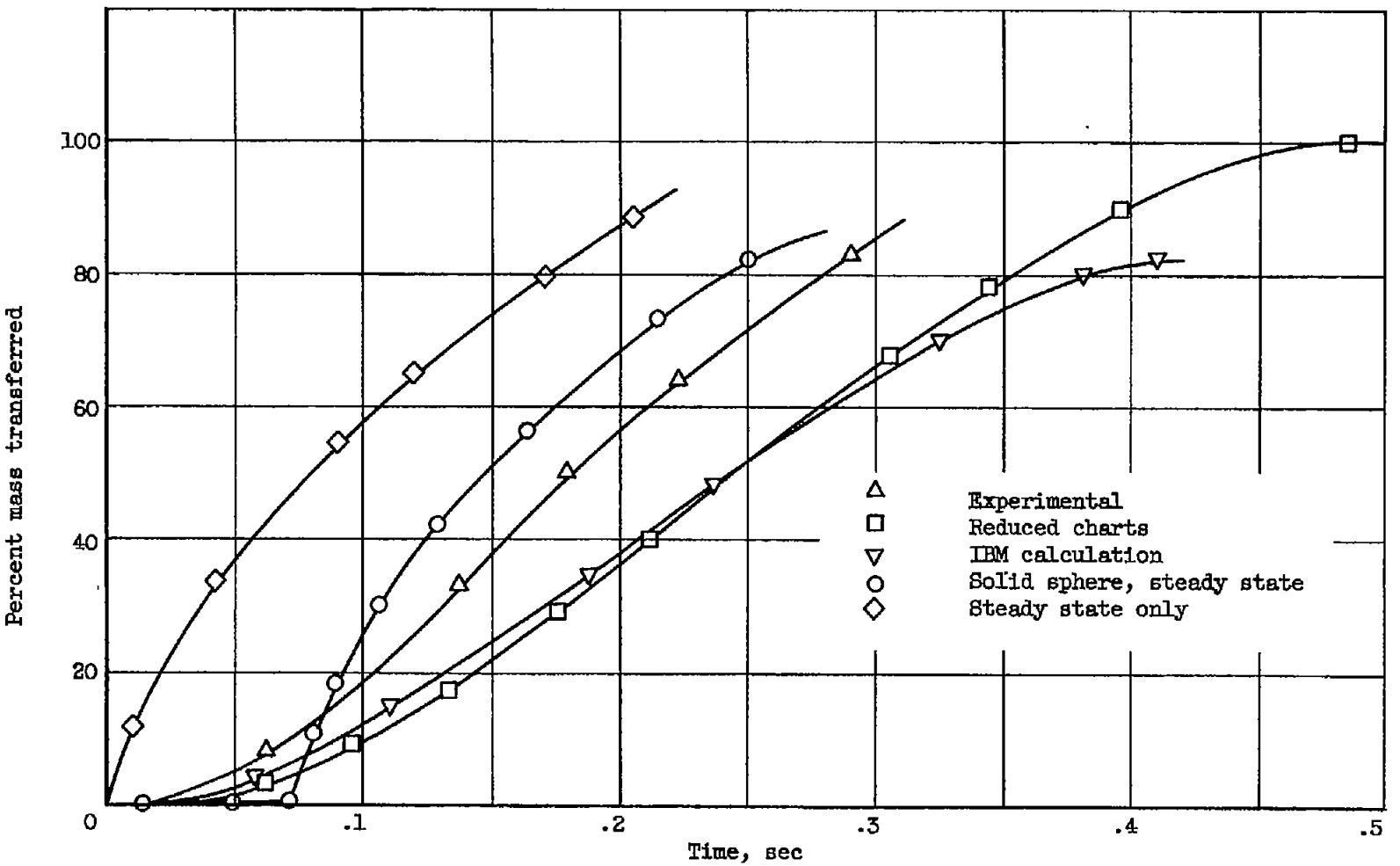

(a) Total pressure, 1 atmosphere absolute; air temperature, 1280° R; air velocity, 120.9 inches per second; initial radius, 0.108 inch; initial liquid temperature, 612° R.

Figure 14. - Comparisons of various calculations with experimental data for n-decane.

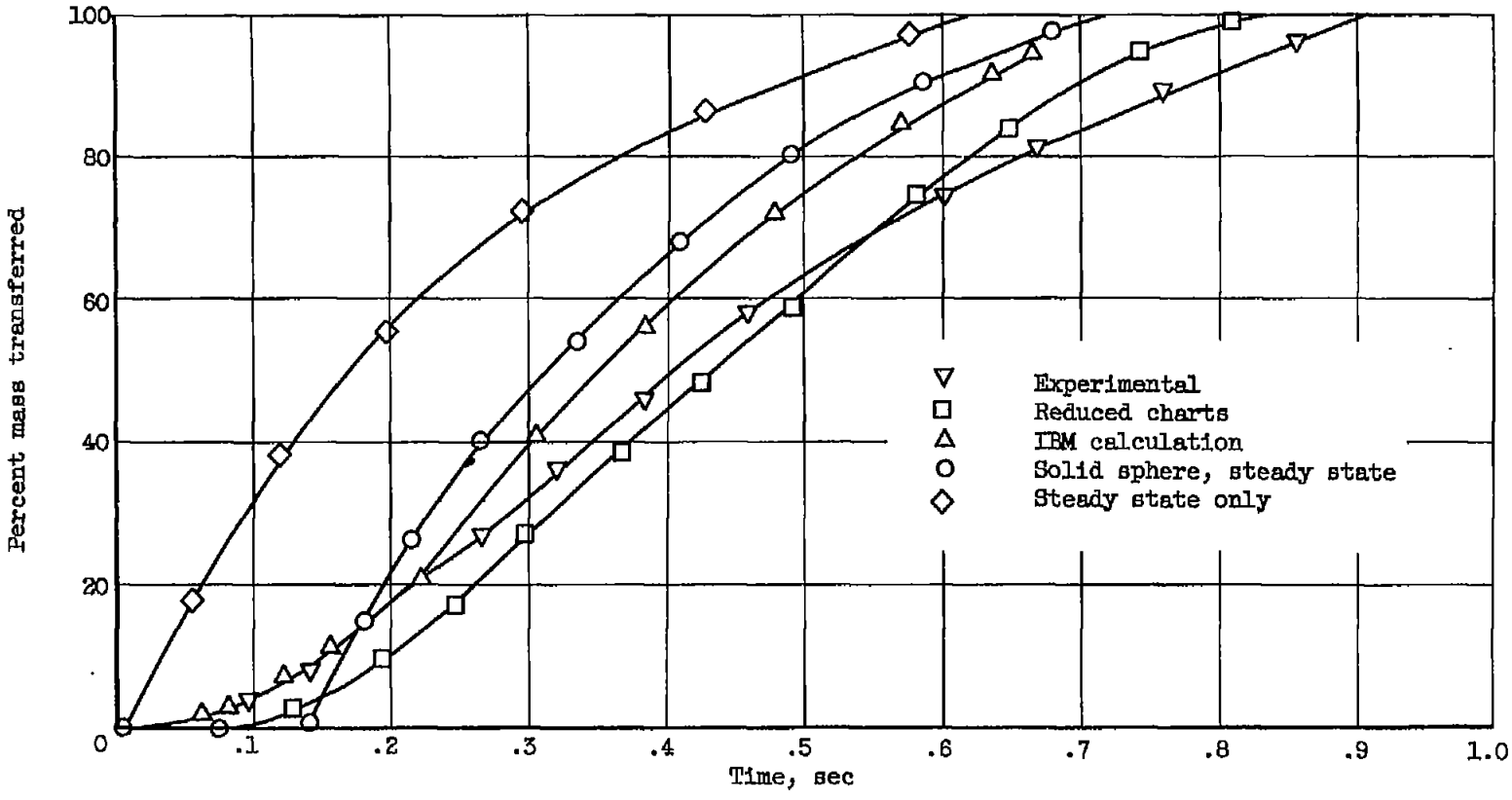

(b) Total pressure, 1 atmosphere absolute; air temperature, 1040° R; air velocity, 97 inches per second; initial radius, 0.0107 inch; initial liquid temperature, 575° R.

Figure 14. - Continued.

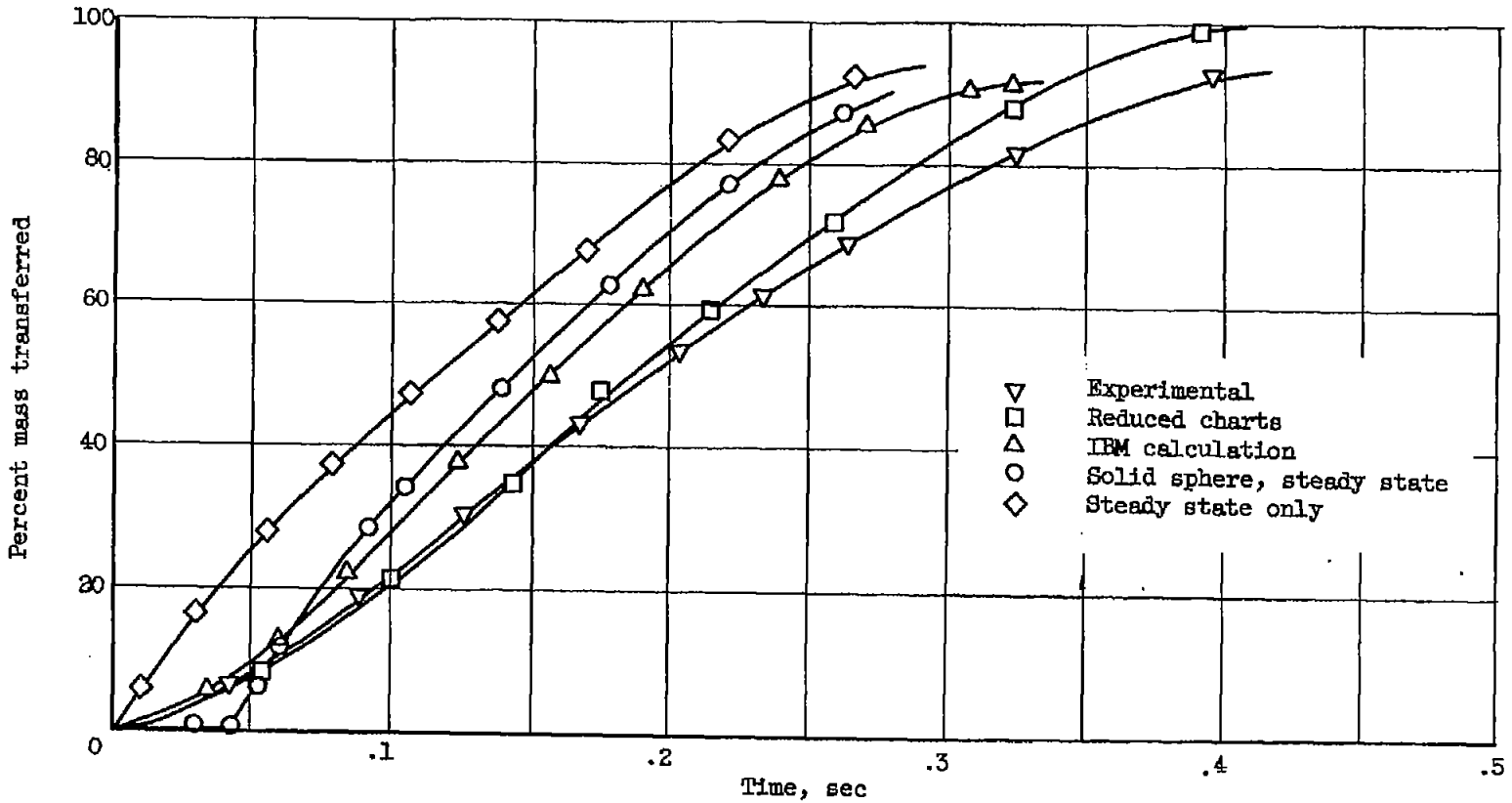

(c) Total pressure, 1 atmosphere absolute; air temperature, 1380° R; air velocity, 101.4 inches per second; initial radius, 0.0102 inch; initial liquid temperature, 650° R.

Figure 14. - Concluded.

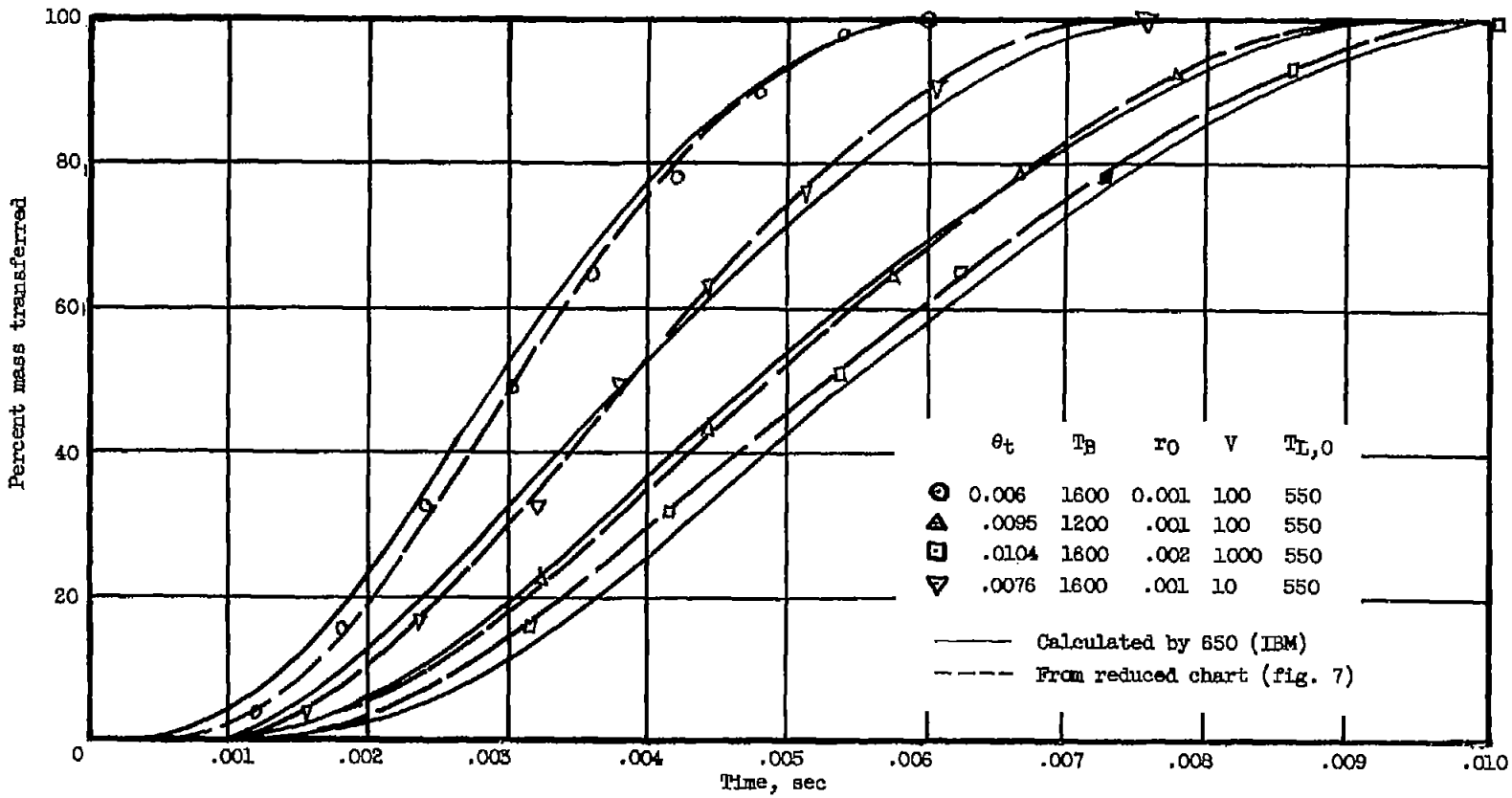

Figure 15. - Comparison of histories obtained from (fig. 7) reduced-variable plot with IBM calculations.

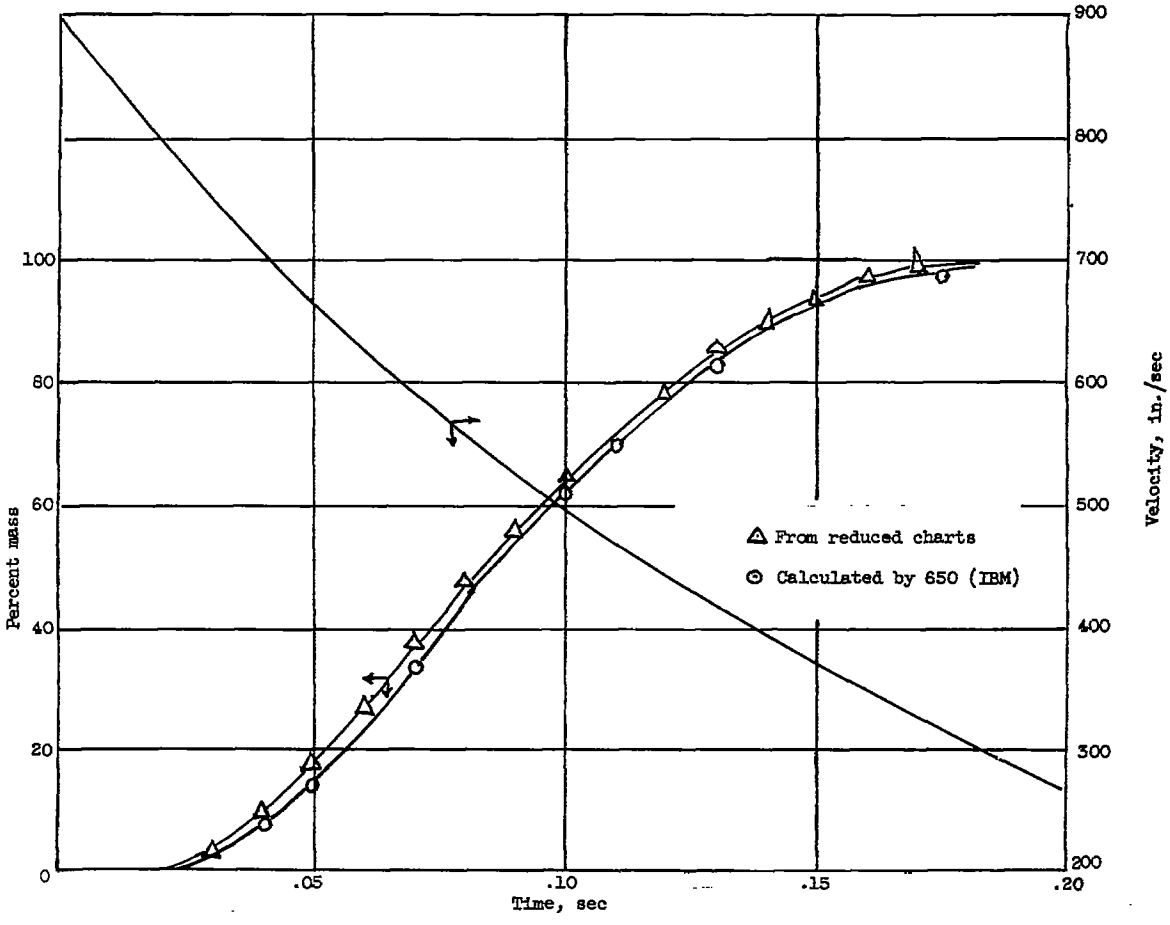

(a) Air velocity, 900 $e^{-6\theta}$; initial radius, 250 microns.

Figure 16. - Comparison of reduced charts and IBM calculations for n-decane droplet with variable air velocity. Total pressure, 1 atmosphere absolute; air temperature, 1600° R; initial liquid temperature, 550° R.

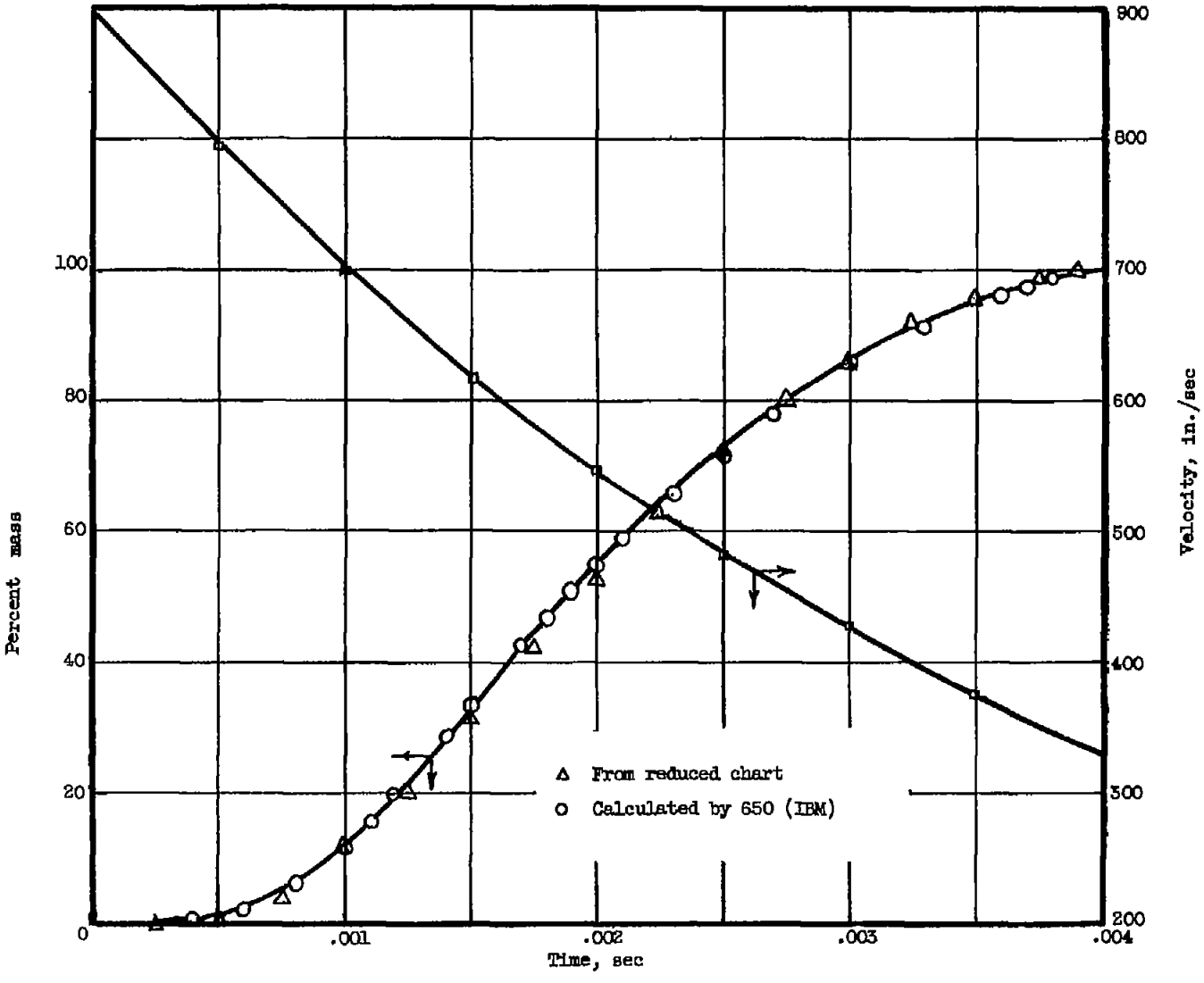

(b) Air velocity, 900 $e^{-2500\theta}$; initial radius, 25 microns.

Figure 16. - Concluded.

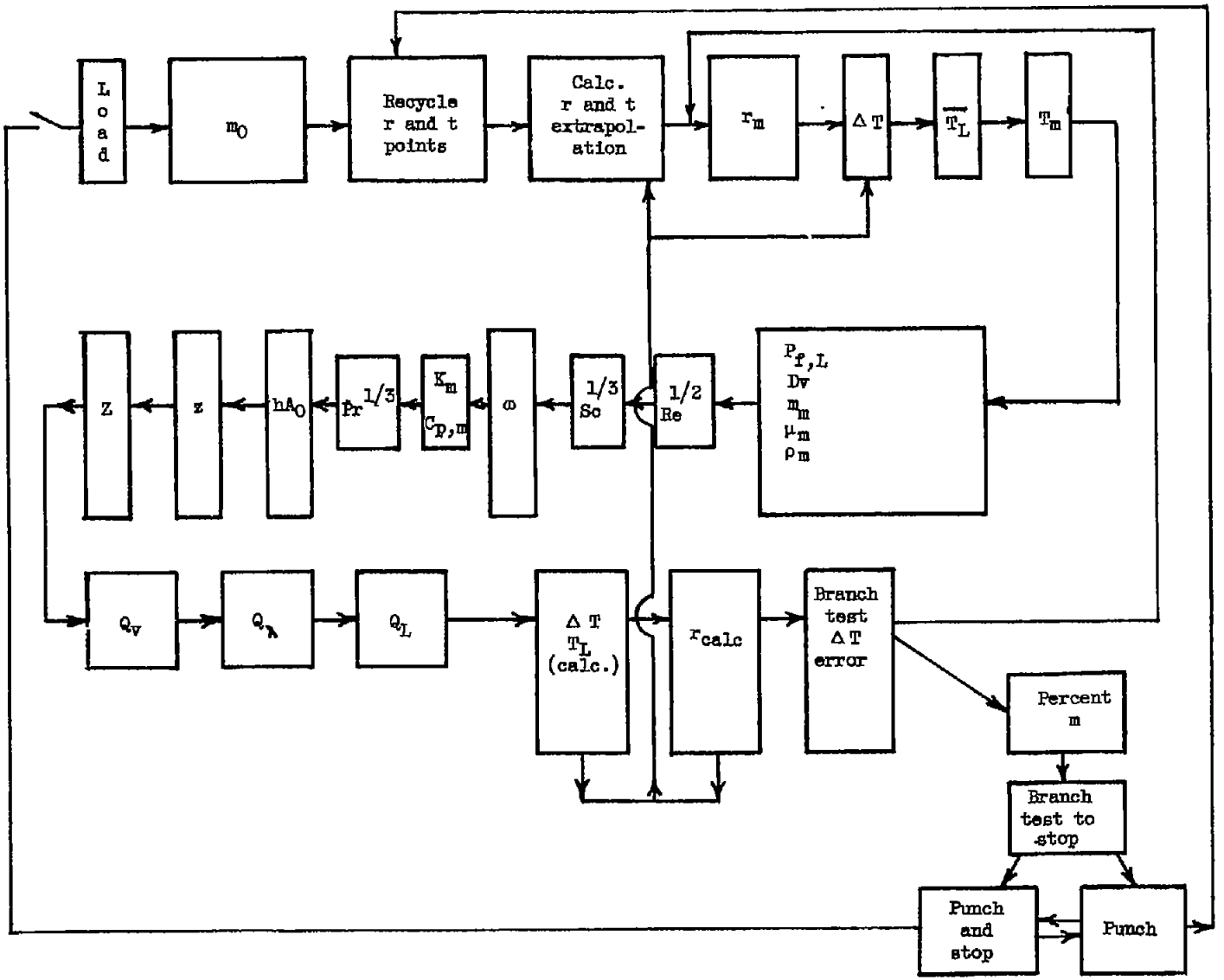

Figure 17. - Flow diagram of IBM 650 program for vaporization calculations.

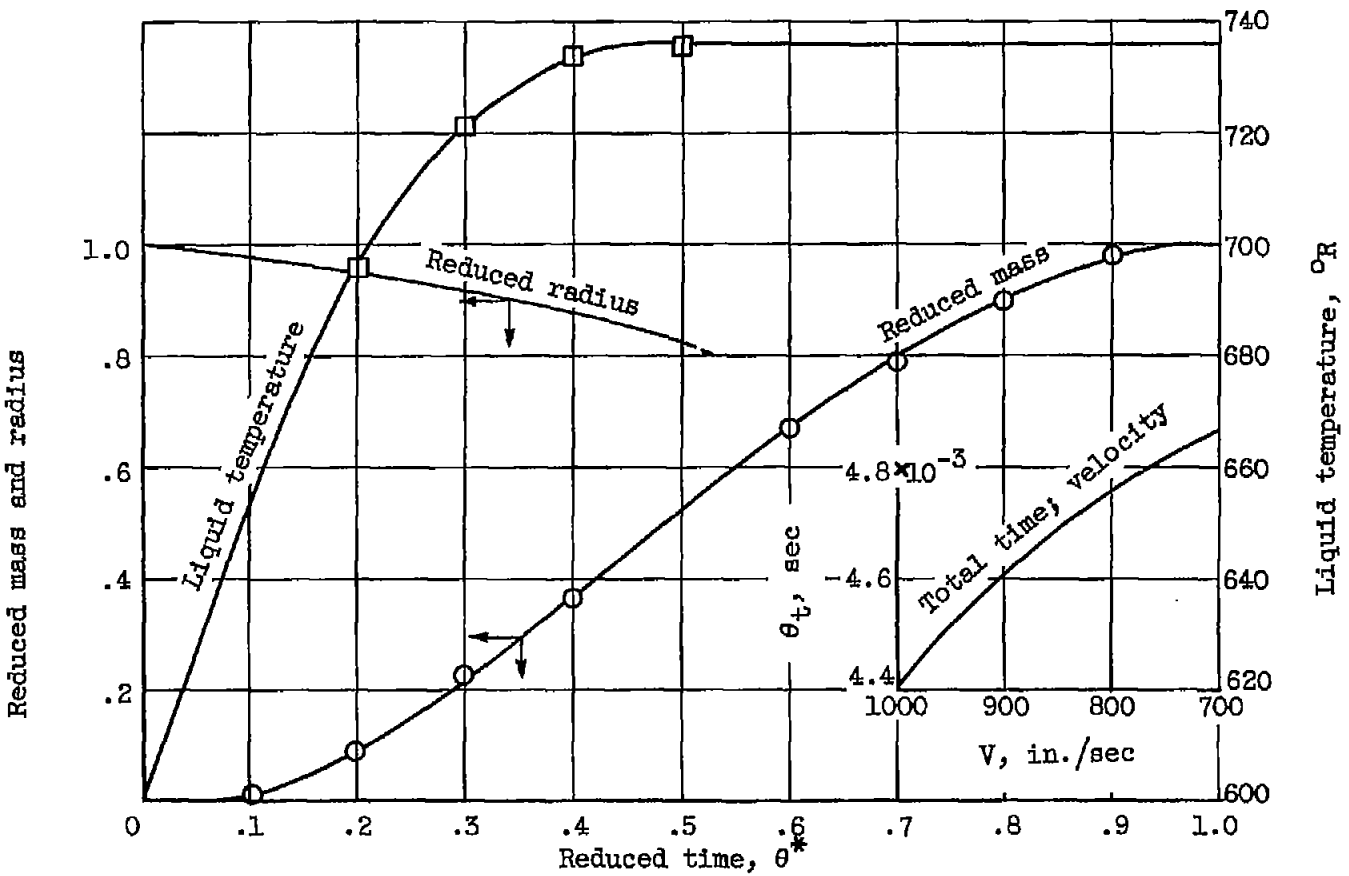

Figure 18. - Temperature, mass, radius, and velocity curves used in sample calculation of appendix C.